A TRIDENT SCHOLAR PROJECT REPORT

NO. 410

Integration of Carbon Fiber Composite Materials into Air-Cooled Reciprocating Piston Engines for UAV Applications

by

Midshipman 1/C Mark E. Trunzo, USN

UNITED STATES NAVAL ACADEMY
ANNAPOLIS, MARYLAND

USNA-1531-2

REPORT DOCUMENTATION PAGE

Form Approved
OMB No. 0704-0188

1. REPORT DATE *(DD-MM-YYYY)*	2. REPORT TYPE	3. DATES COVERED *(From - To)*
04-05-2012		

4. TITLE AND SUBTITLE
Integration of Carbon Fiber Composite Materials into Air-Cooled Reciprocating Piston Engines for UAV Applications

5a. CONTRACT NUMBER

5b. GRANT NUMBER

5c. PROGRAM ELEMENT NUMBER

6. AUTHOR(S)
Trunzo, Mark Evan

5d. PROJECT NUMBER

5e. TASK NUMBER

5f. WORK UNIT NUMBER

7. PERFORMING ORGANIZATION NAME(S) AND ADDRESS(ES)

8. PERFORMING ORGANIZATION REPORT NUMBER

9. SPONSORING/MONITORING AGENCY NAME(S) AND ADDRESS(ES)
U.S. Naval Academy
Annapolis, MD 21402

10. SPONSOR/MONITOR'S ACRONYM(S)

11. SPONSOR/MONITOR'S REPORT NUMBER(S)
Trident Scholar Report no. 410 (2012)

12. DISTRIBUTION/AVAILABILITY STATEMENT
This document has been approved for public release; its distribution is UNLIMITED

13. SUPPLEMENTARY NOTES

14. ABSTRACT

The development of a lightweight, air-cooled, reciprocating engine capable of offering lower fuel consumption provides a viable alternative to small gas turbine engines in UAVs. Composites offer the capability to reduce weight and maintain component strength. Using temperature and strain data, carbon fiber components have been successfully designed to withstand the engine operating conditions while reducing weight and improving UAV performance.

15. SUBJECT TERMS
omposite, Engine, Air-Cooled, Crankcase, Connecting Rod, Carbon-fiber, Carbon-fiber Reinforced Plastic, UAV

16. SECURITY CLASSIFICATION OF:			17. LIMITATION OF ABSTRACT	18. NUMBER OF PAGES	19a. NAME OF RESPONSIBLE PERSON
a. REPORT	b. ABSTRACT	c. THIS PAGE		74	19b. TELEPHONE NUMBER *(Include area code)*

U.S.N.A. --- Trident Scholar project report; no. 410 (2012)

Integration of Carbon Fiber Composite Materials into Air-Cooled Reciprocating Piston Engines for UAV Applications

by

Midshipman 1/c Mark E. Trunzo
United States Naval Academy
Annapolis, Maryland

_____
(signature)

Certification of Adviser(s) Approval

Associate Professor Patrick Caton
Mechanical Engineering Department

_____
(signature)

_____
(date)

Associate Professor Joel Schubbe
Mechanical Engineering Department

_____
(signature)

_____
(date)

Acceptance for the Trident Scholar Committee

Professor Carl E. Wick
Associate Director of Midshipman Research

_____
(signature)

_____
(date)

USNA-1531-2

ABSTRACT

The United States Navy (USN) has shown an interest in the development of small displacement, reciprocating piston diesel engines for Unmanned Aerial Vehicles (UAVs). These engines avoid the logistic challenges of relying on gasoline-fueled UAVs, and have relatively low fuel consumption, but suffer from poor power-to-weight ratios. Reducing weight is of significant importance to UAVs to allow sufficient range and loitering times. Carbon fiber composites offer **strength-to-weight** benefits over the metal components currently used in piston engines. However, composite components have more restrictive operating temperatures. None of the known previous efforts aimed at integration of composites into engines has focused on air-cooled engines and on their potential benefits for UAVs. A small, single-cylinder air-cooled gasoline engine was chosen as a convenient test platform and surrogate for an air-cooled UAV engine. The crankcase and connecting rod from this engine were redesigned using a high percentage of carbon fiber in order to reduce weight. To develop the designs, steady-state temperature profiles were measured both internally and externally. The steady state temperatures for the crankcase ranged between 93°C and 150°C while the connecting rod ranged between 120°C and 160°C. Carbon fiber composite test specimens were tested for strength at a comparable range of temperatures to demonstrate thermal viability. The tensile tests proved the carbon fiber to be comparable to all aluminum material properties, if not better. These data enabled development of a thermal model to enable prediction of expected temperatures with variable amounts of carbon fiber integration. Stress was modeled on the stock engine at the worst-case operating condition and used to design the composite crankcase and connecting rod to ensure sufficient strength to survive at this extreme condition. The modeled stresses resulted in a factor of safety of at least 1.5 for the connecting rod and 3.8 for the crankcase. No attempt to measure stresses experimentally on the stock engine were successful, although lessons learned here could assist future experimentation. These composite components were integrated and tested successfully, for various lengths of time, on the engine and indicate a potential weight savings of approximately 80% for the crankcase and 26% for the connecting rod. The composite case failed after approximately 20 minutes ($O(10^4)$ cycles) of operation at the best torque condition (worst-case in terms of mechanical stress) due to manufacturing deficiency at the corners and base; the connecting rod failed after approximately 2.5 minutes ($O(10^3)$ cycles) of worst-case operation due to a failed bearing that was slightly (~0.001 in) undersized. Neither failure was a predicted-mode, and could easily be remedied with further time and iteration.

Key Words: Composite, Engine, Air-Cooled, Crankcase, Connecting Rod, Carbon-fiber, Carbon-Fiber Reinforced Plastic, UAV

Acknowledgements

This project has received a great amount of support throughout its duration. It has been one of the most challenging academic experiences of my academic career so far and would not have been possible without the knowledge, skill, and patience of those listed below. I would like to express my gratitude for everything they have helped me accomplish.

Machine Shop
- Tom Price
- Brandon Stanley
- Matt Stanley
- Mike Superczynski
- Andrew Pullen
- Jesse Baldwin
- Gary Gibson

Engines Lab
- Charlie Baesch
- John Hein

Associate Professor Patrick A Caton
Associate Professor Joel Schubbe
Associate Professor Steve Graham

Table of Contents

List of Figures

List of Tables

List of Symbols

α: ..... Percent Change in Aircraft Weight

ATC: ……..…….After Top Center

β: .....Percent Change in Aircraft Range

CAD: ……..……Crank Angle Degree

CFRP: ……..……..Carbon Fiber Reinforced Plastic

$\Delta range$: ..... Change in Aircraft Range

ΔW_{engine}: ..... Change in Engine Weight

EES: ……..…..…….Engineering Equation Solver

ε: ..... Percent Change in Engine Weight

η: ..... Engine Weight as a percentage of Aircraft Weight

FEA: ……..…….Finite Element Analysis

FS: .....Factor of Safety

G10: ……..…….Fiberglass Composite

MMC: ……..……..Metal Matrix Composite

OHC: ……..……...Overhead Camshaft

$\dot{Q}$: ….....Overall Net Heat Transfer

r: .....Decrease in Maximum Range with an Increase in Payload (nm/lbm)

r*: ..... Normalized r using Maximum Range and Empty Aircraft Weight

RPM: ……..…....Revolutions per Minute

RTV: ……..……Room-Temperature Vulcanizing Gasket Material

TDC: ..... Top Dead Center

1 Introduction and Background

This study focuses on the redesign, development, and fabrication of a composite engine for use in Unmanned Aerial Vehicles (UAVs), and more specifically, small UAVs. UAVs have many tactical advantages over a conventional manned aircraft which include lower fuel consumption, sustained surveillance of the battle space, and the ability to be deployed by soldiers on the ground. The Naval Research Laboratory has produced battery powered and small turboshaft engines and is currently testing the performance of these engines [5]. However, the Department of Defense (DoD) and the U.S. Navy (USN) have recently become interested in developing small UAV diesel engines in an effort to move toward engines that efficiently utilize heavy fuels (i.e. diesel fuel or jet fuel). The higher **flash point** of heavy fuels makes storing them onboard naval vessels safer. Heavy fuels are also more common for their use in aircraft and to power onboard engines and generators, making them readily available to forces forward deployed.

An engine that is capable of serving in an aviation based capacity must have a high **power to weight ratio**. Gas turbines have very high power to weight ratios which explains why most commercial and large private aircraft are powered by a gas turbine of some sort, whether it be a turbo prop, turbo fan, or turbo jet. Figure 1 shows the **power density** (power per unit weight, hp/lbm) versus the brake power output of 44 engines, separated by class: gas turbine; air-cooled gasoline; and air-cooled diesel engines. Note that gas turbine engines sit at the top of the graph in terms of power-to-weight and have a wide power range making them viable for many different applications, large or small. Gasoline engines come close to the power-to-weight ratio of gas turbines and are capable of serving in small power applications such as a small UAV, however the utilization of heavy fuels is desirable due to their availability and the increased safety involved with storing them. Diesel engines are at the bottom of the graph with poor power-to-weight ratios due to high engine weight. Notice on Figure 1 that there is a natural delineation between those engines that are originally purposed for aviation and those, including some of the gasoline and almost all of the diesels, that were included in the figure but are not originally intended for aviation. However, one diesel engine sits above the line and is more similar to the other aviation engines on the figure. This diesel is a specialty engine developed by Cosworth for the USN. Figure 1 may suggest that the pursuit of diesel use in small UAVs may not be worthwhile because small gas turbines can be used instead with much higher power density. They use heavy fuels and have high power to weight ratios making them great candidates for UAVs.

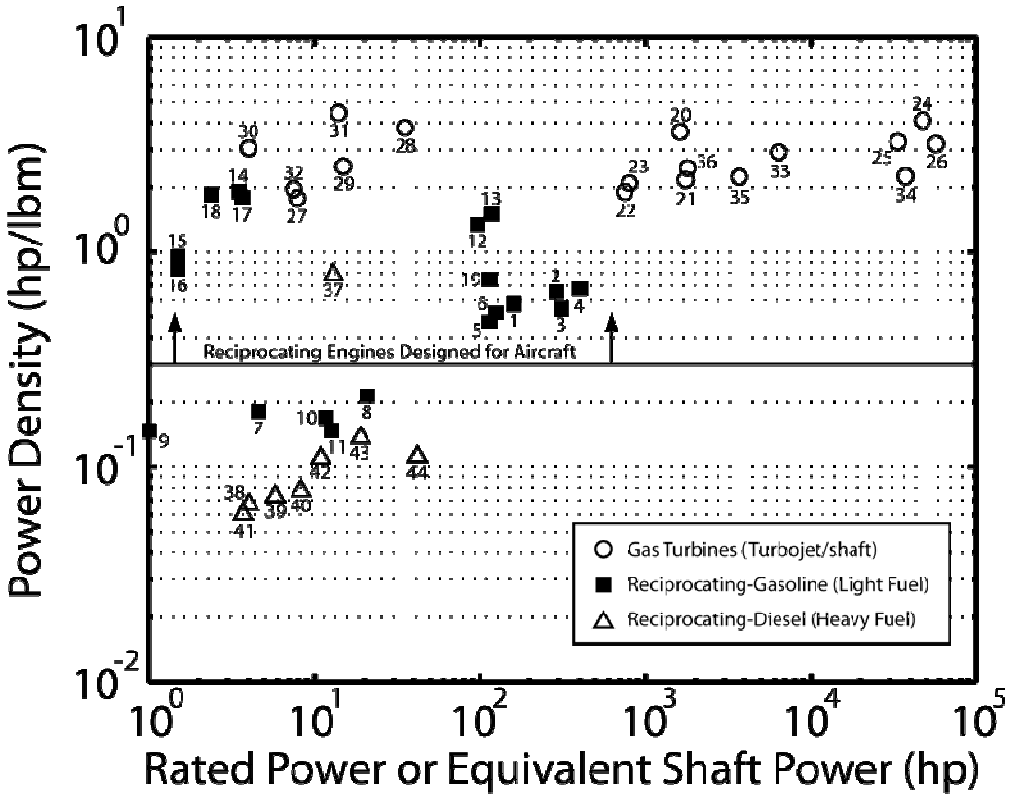

Figure 1: Power Density of Various Engine Types Compared to the Engine Power Output

The problem with using gas turbines in small power applications is that as gas turbines decrease in size they become relatively inefficient. This trend is shown in Figure 2 where the high powered gas turbines are just as efficient as a diesel or gasoline engine, but the smaller gas turbines become terribly inefficient. The larger gas turbines have great power to weight ratios and are efficient. Therefore they make a great choice for use in aviation. However, the poor efficiency of small gas turbine engines means that mission times of small UAVs would greatly be decreased. This is undesirable considering the fact that a longer loitering time gives a greater tactical advantage to forces on the ground. Figure 2 shows that diesels are capable of providing far better efficiency (logarithmic vertical axis) at small power outputs.

The use of composites in small diesel engines therefore offers the potential to improve the poor power-to-weight ratio of heavy-fueled (diesel) engines, making their use in UAVs far more attractive. Diesels clearly have the efficiency required to give UAVs an acceptable time on station but they lack the power to weight ratio required for use in aviation. By decreasing the weight, thereby increasing the power to weight ratio, more diesels will be able to cross the line into aviation applications. Although this study aims to provide the first prototype designs for composite components in diesel engines, a single cylinder gasoline engine was chosen as a convenient test platform for low cost and simplicity for integrating composite components (overhead cam and valve, diagonally split crankcase). These factors allowed components to be partially replaced with composites to test their performance in an elevated temperature environment.

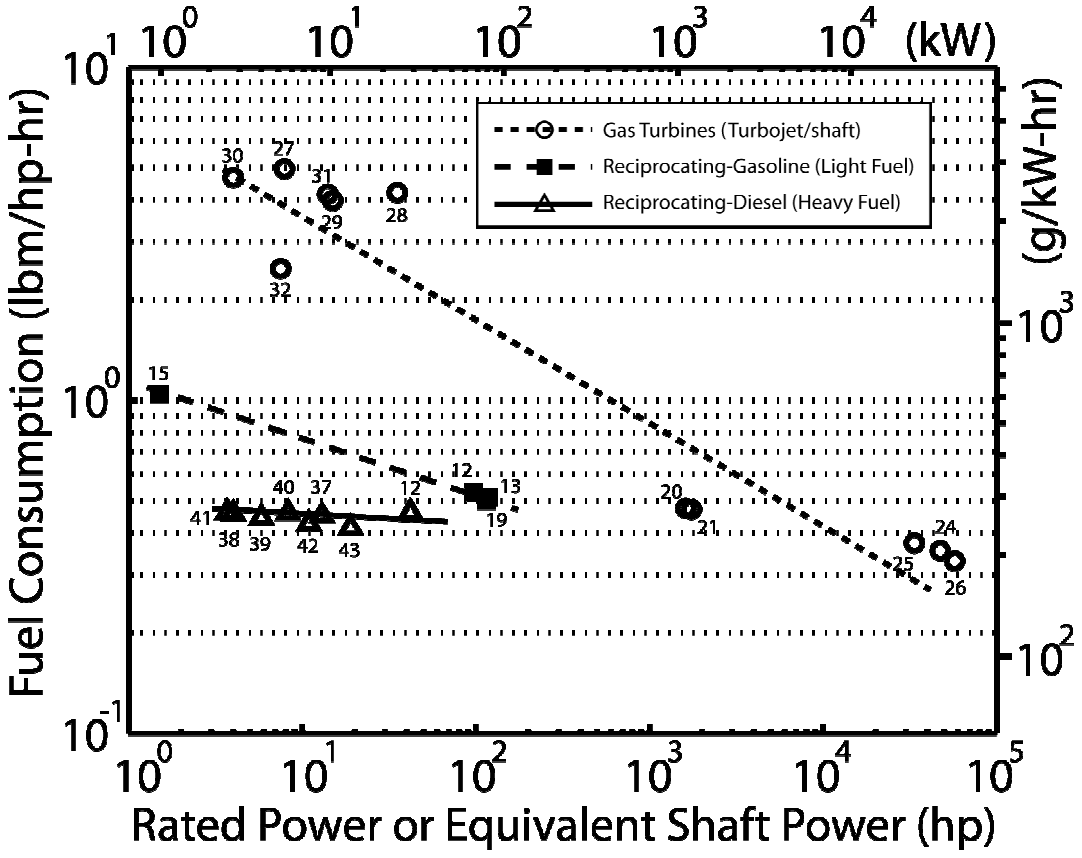

Figure 2: Fuel Consumption vs. Power Output for Various Engine Types

A composite can be defined as a combination of a matrix material (often a resin) cured within a reinforcing material (often fibers). The resin matrix material binds the fibers in a fixed orientation, distributes loads across the fibers, and protects them from the environment. The reinforcing material (fibers) then serves to carry the majority of the load. One everyday composite material is concrete reinforced by metal rebar. The rebar acts as the "fiber" held together in the matrix of the concrete. While reinforced concrete is not an ideal composite for use in UAV engine development, other composites, such as carbon fiber, do provide comparable strength to steel or aluminum while providing significant weight savings.

The strength of a composite depends heavily on the orientation of the fibers relative to the direction of loading. A +/-45° orientation indicates that the fibers are 45° to the load. A 0°-90° orientation indicates that 50% of the fibers are in the direction of the load while 50% are perpendicular to the load. Ideally, the load will act in the longitudinal direction of the fibers so that the fibers bear the load instead of the reinforcing material. However, in an application such as a diesel engine, the load will not act only in one direction. A layup indicates how the composite is fabricated, including the orientation of the fibers which is illustrated in Figure 3. A quasi-isotropic layup addresses the issue of loading in multiple directions. The fibers used in a

composite are available in sheets and the matrix is then added to the fibers. The orientation of the fibers is changed layer by layer so that fibers travel in several directions throughout the material. This allows the composite to bear load in multiple directions. The composite material must then be cured in order to make the material structurally sound. This is done by applying heat and both positive and negative pressure (e.g. vacuum), using a technique known as vacuum bagging.

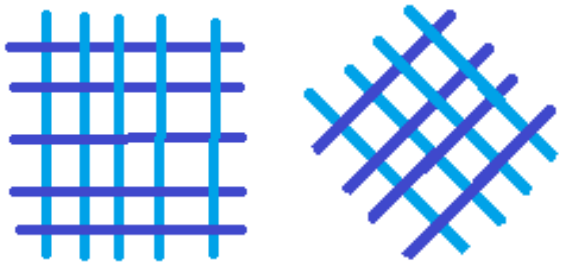

Figure 3: Orientations of Fibers 0°-90° (left) and +/-45° (right)

There have been few past efforts aimed at integrating non-traditional plastic or composite components into reciprocating piston engines. Polimotor Research Inc. (Matti Holtzberg, Fair Lawn, NJ) worked extensively on gasoline engines constructed with significant plastic components in the 1970s and 1980s. Their work involved a high-strength thermoset plastic, called Torlon, which used injection molding to create the components. The engine was used in a gasoline application and it modeled the 2.3 Liter 4 cylinder engine of the Ford Pinto. The block, piston skirts, connecting rods, oil pan, and most of the cylinder head was made from Torlon and proved to be capable of surviving under the loads of an engine.

The standard Ford Pinto motor made of metal components produced 88 horsepower and weighed 415 pounds. By the time Holtzberg created a second generation Polimotor two years later, it made 300-horsepower and only weighed 152 pounds [2] [7]. The gasoline plastic motor clearly has advantages over the standard metal component engine with large weight savings. Holtzberg's work represents the limited development that has occurred in engines with composite components, and his work has not progressed to the diesel application.

While Polimotor was the most extensive and complete attempt to make a composite engine, other attempts in the field do exist from the 1980s. Honda was the first company to pursue a metal matrix composite (MMC) connecting rod using steel fibers in an aluminum matrix [2]. Toyota designed a piston crown reinforced with alumina and carbon fibers [2]. Western Michigan University continued work with their injection molded 2-stroke engine using chopped graphite fibers for reinforcement. Replacing the stock block, head, and cylinder sleeve, they claimed weight savings of 40% [2]. These endeavors involved injection molding or some form of a metal matrix, but they did achieve significant weight savings.

In the 1990s NASA Langley began to research carbon-carbon composite pistons for use in internal combustion engines. This study focused not only on survival of the part, but on efficient manufacturing as well. Initial cost per carbon-carbon piston was $200 compared to a $5 aluminum piston [2]. After the manufacturing process had been streamlined, mass production costs of carbon-carbon pistons was reported to be down to $5 making it a direct competitor with

aluminum [2]. The 1990s also witnessed work from Volkswagen to develop composite connecting rods. Titanium bearing surfaces and compression plates were used with a composite perimeter to handle tensile loads [2]. The study found that manufacturing processes were too difficult to pursue further.

The Volkswagen study concluded that temperature effects on composite replacements for metal components were marginal. However, this conclusion was assuming proper oil lubrication and engine cooling in a water-cooled engine [1]. The study did acknowledge that the oil and fuel contacting the resin in the composite may cause problems, and that the contact between steel and composite potentially poses a galvanic corrosion issue [1]. The study concluded that in a water-cooled engine, fiber composite material could effectively replace steel components. A similar Russian study demonstrated a 30% weight reduction using a composite material to replace the stock steel connecting rod and a 3dB noise reduction was observed [4]. This 30% weight reduction was repeated in a study conducted by Daimler Benz. Daimler Benz replaced the steel connecting rod of an M 102 engine with carbon fiber reinforced plastic [6]. These previous studies dealt with the replacement of steel components in water-cooled engines used in automobile applications.

These previous efforts, while few in number, do indicate the potential for various forms of composites to replace traditional metal components in reciprocating piston engines. These efforts also point to the importance of thermal design, but none of these studies utilize an air-cooled engine, likely to be utilized in a small UAV application. The thermal environment of an air-cooled engine could be substantially different than that of a water-cooled automotive engine. Also, none of these few previous studies considers the potential for composites within UAV applications. The objective of this study is to reduce the weight of a small, air-cooled reciprocating piston engine by replacing a significant portion of the metal in two important components with carbon fiber reinforced plastics. The two components chosen for composite replacement were the crankcase and connecting rod. The crankcase can form a substantial portion of the weight of an engine, and, since it is often isolated from the combustion event, it endures relatively lower temperatures and stresses. Therefore, the crankcase is an attractive candidate for composite replacement. In contrast, the connecting rod composes a relatively small portion of the engine mass, and for a single-cylinder engine, composes an almost negligible fraction of the total weight. However, the connecting rod will have an increasing weight fraction as the number of cylinders increases. More importantly, the connecting rod is a reciprocating mass directly connected to the piston; by lowering connecting rod mass, the engine can often operate at significantly increased rotational speeds, greatly enhancing the power output potential of the engine.

2 Manufacturing

Synthesis of hybrid materials manufacturing processes, sometimes not fully compatible, became a significant portion of this study as it progressed through the early model stages to the fitment stages. This section aims to describe the manufacturing processes pursued and will detail the rationale for various manufacturing choices and lessons learned, which can inform follow-on work.

2.1 Crankcase Manufacturing

2.1.1 Mold Creation

The crankcase manufacturing process required that a general shape of the Carbon Fiber Reinforced Plastics (CFRP) component be decided upon to begin creating a **mold**. The decision was made that maintaining the shape of the stock crankcase would allow for a fairer comparison between CFRP and aluminum. Once the shape was fixed, a male mold was created using high density foam, representing the crankcase's negative space. The CFRP was then draped over this male mold before being cured. Figure 4 shows the initial, rough mold, in the intended shape of the crankcase, prior to finish-sanding.

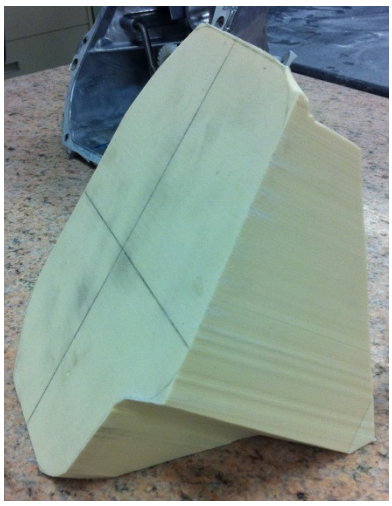

Figure 4: Crankcase High Density Foam Mold Prior to Shaping

High density foam offered a quick, easy, and reliable way to create a mold for a larger object such as the crankcase. Using aluminum as an alternative would have required significantly more time and effort to create the mold. To achieve the rough shape shown in Figure 4, a foam block was cut using a band saw along one plane of the shape at a time. Then, the mold was sanded down to the exact shape, mounted on a board of PVC, and then primed, as shown in Figure 5. The finished mold is reusable and will allow cured CFRP to reliably release from the mold without sticking.

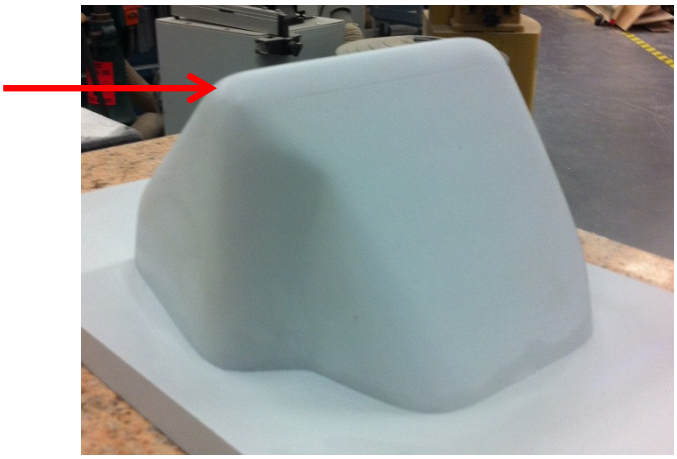

Figure 5: Shaped, Mounted, and Primed Mold for the Crankcase with Weak Spot Annotated

2.1.2 Crankcase Prototype Layup and Cure

A **wet layup** was chosen for the crankcase mold because of the complex shape of the case. A wet layup begins with a dry carbon fiber weave that is placed over the mold. The dry weave is then wetted out with epoxy, a combination of resin and hardener, which bonds the layers of carbon fiber weave together into a structurally sound object. In Figure 5 the tight corners and sweeping faces are visible. These shapes make the use of **pre-impregnated weaves** difficult because in their pre-cured state they are not as flexible as dry fiber weaves used in wet layups. A pre-impregnated weave is a sheet of carbon fiber and epoxy premixed to the correct ratio of carbon fiber and epoxy. Additionally, continuous fibers would be maintained through the use of a wet layup which maintains strength throughout the faces. A pre-impregnated weave would not have been able to meet the contours of the mold and would have required cutting smaller strips and layering the faces, joining them together along the edges, making much of the strength dependent upon the strength of the seams. As will be shown in the Results section, the crankcase ultimately failed due to low density of fiber at the small radius corners, shown at the top of the mold in Figure 5. In a follow-on design, greater care needs to be taken in layup around these corners, or the mold needs to be altered to reduce the curvature radius at these locations. Alternatively, a 'corded' fiber or other configuration could be used in these tight corners to provide additional reinforcement.

With a layup process selected, the next step in manufacturing the CFRP crankcase involved choosing the method for curing. A wet layup does not require that elevated temperatures be used to cure since the resin used for the matrix material undergoes an exothermic chemical reaction, creating its own heating. The crankcase could have been **vacuum bagged**, a process that uses a pump and a plastic covering sealed around the part to remove any air during the cure process, and left to cure at room temperatures and the strength necessary would have been achieved. However, the use of an **autoclave** offers the capability to raise the temperature, allowing for the excess resin to flow more easily through the fibers, and for excess resin to be absorbed during the curing process. Increasing the amount of fibers relative to the matrix resin provides greater

strength and reduced weight (strength to weight ratio) and a thinner part. Also, the autoclave can apply an external pressure on the vacuum bag while it is simultaneously being evacuated, effectively increasing the net pressure difference used during curing.

Two prototype crankcases were produced using this mold. While both used a wet layup procedure, the first prototype was cured at room temperature, not using an autoclave. This first prototype produced a crankcase that weighed 0.55 lbf compared to the stock 2.5 lbf, a 78% weight savings, prior to installing the bushing and machining all necessary holes. However, the radius of curvature around the connecting flange proved to be slightly too large for bolts to seat correctly when securing the case to the rest of the engine.

The second prototype utilized the autoclave at slightly elevated temperature (36°C) and with a net differential pressure of 2 atm (1 atm of pressure applied and 1 atm of pressure being pulled on the vacuum bag). This manufacturing method allowed more resin to be removed during the curing process and achieved a smaller radius of curvature on the connecting flange. This second prototype weighed 0.41 lbf, a further 25% savings over the first prototype, and a total weight savings of 84% relative to the stock aluminum crankcase. The tighter radius along the flange made it possible to drill the bolt holes correctly and properly secure the case to the upper portion of the engine. The bolt pattern along the flange was drilled using a standard drill press and all excess flange material was cut away to improve the weight savings. Thus, the autoclave is recommended whenever possible to achieve the desired geometry and weight savings.

2.1.3 Crankcase Bearing Attachment and Alignment

With the crankcase prototype created, two big challenges remained. First, how to properly insert the crankshaft bearing into the side of the carbon fiber case. Second, how to ensure that this bearing was accurately aligned with the opposing crankshaft bearing once the CFRP case half was attached.

Addressing the first issue, several designs to install a bushing on the CFRP case were considered. The initial design called for building up a thick pad of CFRP material on the bearing face shown in Figure 6 to create enough thickness for a metal bushing to be supported. By drilling an oversized hole through this CFRP pad, the bushing would be set in with a rubberized sealant material, such as **a Room-Temperature Vulcanizing (RTV) gasket-making paste,** , which would allow working time for the bushing to be aligned perfectly by assembling the crankshaft in the engine, allowing the crankshaft to self-align the bushing in the RTV before it set.

However, this approach was ultimately abandoned due to the amount of excess CFRP that would be added to the load bearing face. Furthermore, the stock engine bushing included complex lubrication geometry that allowed for a film of oil to remain on the bearing surface for bearing lubrication. This geometry would be difficult to accurately re-create with the CFRP pad and would be lost if a generic bushing was sealed into the side of the case. Therefore, the stock aluminum bushing was cut from the side of the stock aluminum crankcase, capturing the original stock lubrication geometry. The Honda GC-160 accessory bolt pattern was used to secure the cut bushing to the CFRP case. Figure 6 shows the CFRP case with the attached bushing and oil slinger post.

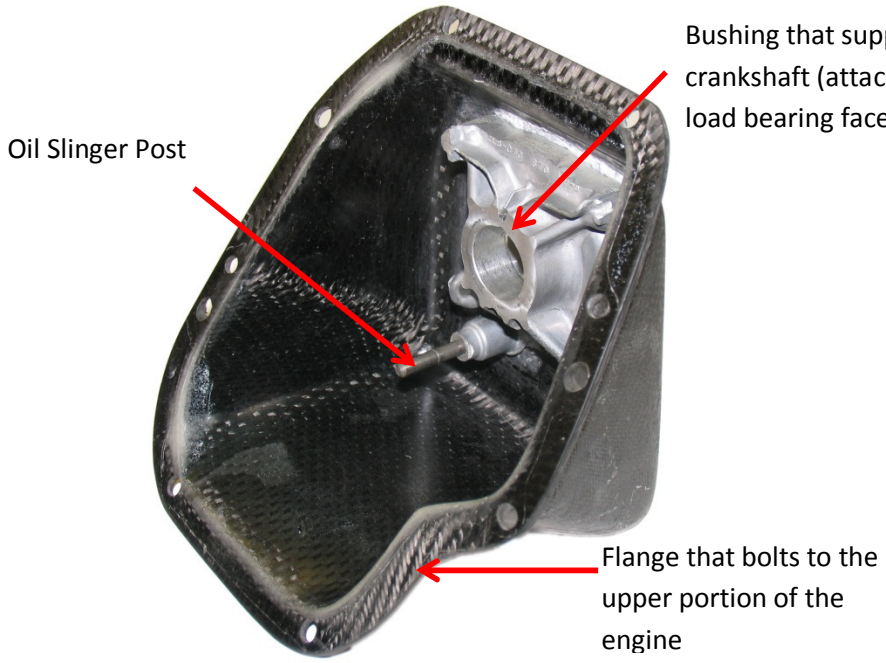

Figure 6: CFRP Crankcase with Attached Bushing and Oil Geometry

The second issue mentioned above, alignment, posed significant manufacturing challenges. For a rapidly rotating shaft, such as the crankshaft in an engine, accurate alignment is paramount. In three-dimensional space, there are six possible degrees of freedom: three coordinate directions (x, y, and z) and the three corresponding rotations above each of these axes. To properly align this aluminum bushing with the paired bushing, two of the coordinate directions and two of the rotations are important, so four total degrees of freedom must be matched. Furthermore, the bushing itself must be secured to the face of the CFRP case, which did not conform perfectly to the surface of the aluminum bushing, neither of which were flat. Also, the CFRP case face was not perfectly parallel with the opposing case face. In short, no pre-alignment with any of the required four degrees of freedom was guaranteed, and steps had to be taken to ensure that each degree of freedom was accurately constrained to enable proper rotation of the crankshaft.

Once the center crankshaft hole was properly cut, locating the aluminum bushing was made simpler. However, maintaining level geometry in the bushing was difficult. The load bearing face of the case was not perfectly parallel with the opposing aluminum face, causing the crankshaft to seize. Moreover, despite using the increased pressure of the autoclave to reduce radii at the edge of adjoining faces, the radius on the load bearing face to the flange proved to be too large to allow the bushing to lay flush. These challenges were met first by grinding the aluminum bushing to the approximate correct surface shape so that it lay approximately flush on the surface of the CFRP case. The four degrees of freedom critical for alignment were all met using a "**liquid shim"** of epoxy between the aluminum bushing and the CFRP face. This liquid shim was a thick pad of epoxy, mixed to be thick enough on application that it would not run out of the gap between the aluminum bushing and CFRP wall. The engine was then assembled with

this epoxy liquid shim in place, allowing the crankshaft itself to ensure alignment in all the required degrees of freedom. As the epoxy liquid shim set, crankshaft alignment was fixed.

Even with the liquid shim, however, fitment problems were still encountered with the thickness of the aluminum bushing. The thickness of the bushing was too large to fit properly and allow for the crankcase to seal properly on the upper portion of the engine. The outward facing edge of the bushing in Figure 6 was cut down to the minimum thickness allowable before the oil slinger post would be lost. To reduce the thickness further, the inward face was cut down and a new oil hole was bored to maintain proper lubrication during operation. These modifications to the stock aluminum bushing allowed for the CFRP crankcase to properly bolt to the upper portion of the engine.

In order to ensure that the CFRP-case engine could be tested on the same dynamometer stand as the stock engine, the proper height and alignment of the crankshaft must be achieved, identical to the stock engine. This represents an additional alignment challenge. The first challenge was to ensure that the crankshaft was aligned with both the aluminum and CFRP faces of the prototype engine. The second challenge was to ensure that the new CFRP prototype engine had exactly the same crankshaft height and alignment as the stock engine. The CFRP crankcase was secured to a fiberglass baseplate that would give the prototype CFRP engine the same height and alignment of the stock engine The fiberglass base was not designed to be considered with the weight reduction calculations because in practical application of the redesigned engine, new engine mounting points would be incorporated into the crankcase design and a specific height would not be necessary. As shown in Figure 7, precision shims were used to bring the crankshaft to a level position that matched the position of the crankshaft in the engine's stock configuration. The base was then epoxied to the bottom of the CFRP case using room temperature curing resin with glass bead filler. With the base mounted to the CFRP case and the stock bolt pattern bored, the crankcase was properly prepared for testing. As will be noted later, the second main failure point of the CFRP-case prototype engine, beside the high radius of curvature corner, was the epoxy joint between the CFRP case and fiberglass base. Little initial attention was given to this joint, as an excess of resin could be used to ensure strength. However, this joint experienced failure in the prototype test, and more significant attention should be paid to the proper design of this joint in follow-on work.

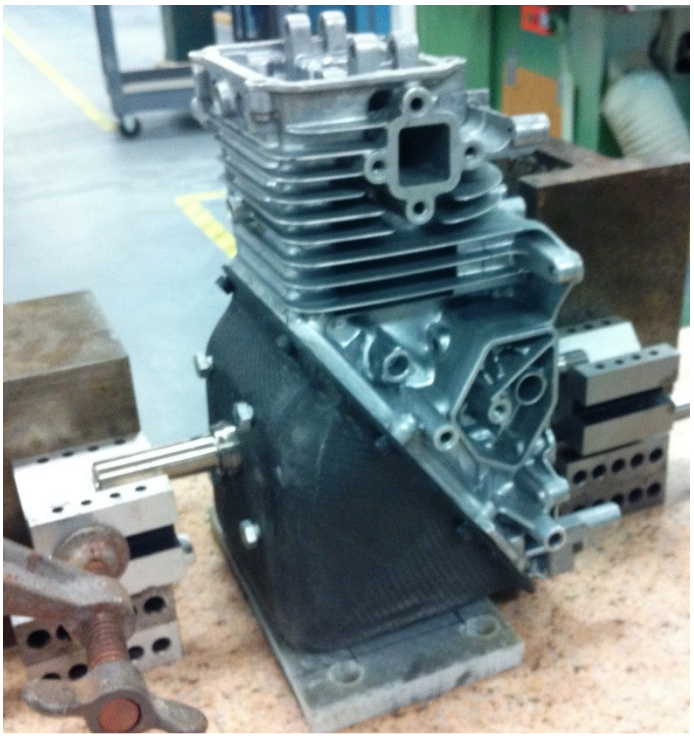

Figure 7: Crankshaft Height Adjustment and Alignment using Precision Shims

2.2 Connecting Rod Manufacturing

The connecting rod manufacturing process benefited from lessons learned in the crankcase manufacturing process. Once again, the first step was to choose a shape and create a mold for the new connecting rod. Like the crankcase, the connecting rod maintained the same profile as the stock connecting rod. However, the reason behind this decision differed slightly. The connecting rod has very tight clearances within the engine so any deviation from the original shape of the aluminum connecting rod could cause catastrophic interferences inside the engine. As will be shown later, a small interference did, in fact, result, but likely did not contribute significantly to the failure of the connecting rod.

The mold for the connecting rod was made from aluminum due to its smaller size and because the shape was amenable to two-dimensional machining (whereas the crankcase required a three-dimensional mold). In addition, aluminum would maintain its original shape better than a high density foam mold, and would allow more elevated temperatures during the curing process. Since the connecting rod was anticipated to experience potentially higher temperatures, greater cure temperatures were desired. Finally, the crankcase mold proved to need repair after the first crankcase was manufactured, and since multiple connecting rods were desired for testing, the aluminum mold offered the potential for greater resilience. One connecting rod would be tested within the engine and the other two were to be used for crush testing at room temperature and then operating temperature. Figure 8 shows the mold split directly down the middle, off axis from the center line of the connecting rod. For follow on work, this would be advised against due to the sharp curves it leaves when trying to fit the uncured connecting rod in the mold. Instead, it

would have been more advisable to use the center-to-center line from bearing surface to bearing surface as the reference line for cutting.

Figure 8: CFRP Connecting Rod Mold

The composite material chosen for the CFRP connecting rod was pre-impregnated carbon fiber. A test plate of unidirectional fibers was created to cut samples out of for tensile testing of the plies that were intended for the connecting rod sides. When manufacturing of this plate was complete, the fibers had begun fraying and tearing apart during the removal of the plate from the autoclave as seen in Figure 9. To counter this fraying, a combination of unidirectional plies and +/-45° weave plies was used. The +/-45° weave holds the unidirectional fibers together, preventing the cured material from coming apart.

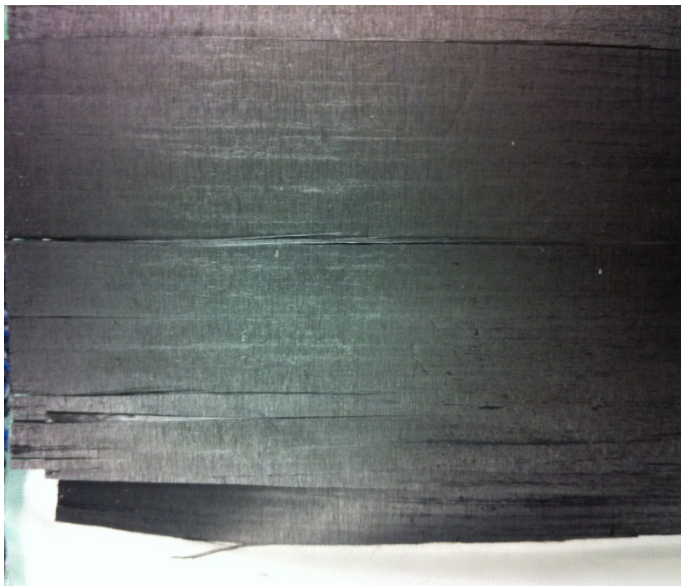

Figure 9: Frayed Unidirectional Test Specimen Plate

A hybrid assembly was chosen for the connecting rod consisting of aluminum coins, G10, and the CFRP. The aluminum coins are solid pieces of aluminum that will serve as bearing surfaces once holes are bored into them. G10 is a fiberglass composite material that can be machined easily and used to give the component stiffness. The connecting rod was cured with all of the pieces in place, rather than dropping the coins into the CFRP loop and doing a post cure to bond the coins and the G10 core. The two aluminum coins, which would have bearing surfaces bored out, and the G10 core were placed together. Then the CFRP was wrapped around the assembly. Foam cutouts held the G10 core on the connecting rod's centerline as shown by Figure 10. The assembly with the CFRP loop was then placed into the mold and the mold was closed using a vise.

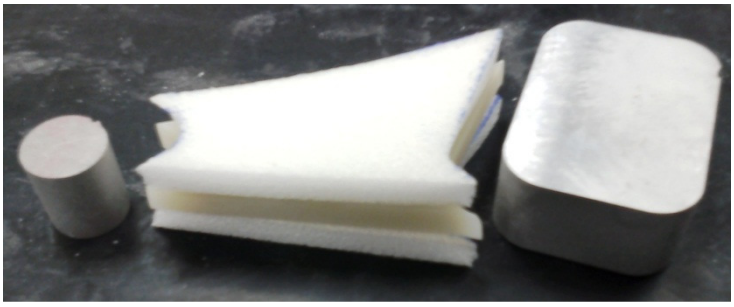

Figure 10: Aluminum Coins (left and right) and G10 Core (in between the alignment foam) Prepared for CFRP Wrapping

Pre-impregnated CFRP unidirectional and +/-45° woven carbon fiber fabric prepreg was used for the loop. Pre-impregnated material was a viable application for the connecting rod because there are no complex geometries for the CFRP to negotiate. Prepreg aids in maintaining proper fiber alignment. Additionally, the pre-impregnated material offers an ideal fiber to resin content ratio, which keeps excess resin from reducing the weight savings. An initial wrap of +/-45° weave was done to ensure that the unidirectional fibers did not separate. The +/-45° weave also served to prevent micro-buckling after curing. The aluminum coins expand more due to a higher coefficient of thermal expansion; therefore, during cooling the coins will contract, pulling the CFRP inward. The +/-45° weave alleviates some residual stress during cooling because the fibers are able to rotate to align during expansion, unlike a 0°-90° weave or unidirectional ply. Five layers of unidirectional fibers were then applied, and then +/-45° weave strips were used on the legs between the coins to increase bending stiffness with additional thickness and to prevent any air gaps in the mold.

The connecting rod was cured in the autoclave due to the anticipated higher temperature requirements of the connecting rod. The recipe for curing was to **debulk**, or remove the air in the vacuum bag, for five hours to remove any excess air between plies, heat to 180°C for two hours, then ramp the temperature back to zero. A 1 atm vacuum was pulled on the part during the entire curing process. Figure 11 shows the connecting rod after the curing process. Notice that all components are bonded together, forming a hybrid material (carbon fiber reinforced epoxy, G10, and aluminum) composite connecting rod.

Figure 11: Hybrid Material Composite Connecting Rod Pre-Machining

The bearing surfaces and end cap were machined after the connecting rod had cured. The wrist pin bearing surface was machined and the center of the crankshaft bearing surface was then located, as per stock connecting rod dimensions. The bolt holes of the end cap were then bored and tapped to prepare the connecting rod for splitting. By machining the bolt holes first, the cap can more accurately be placed back into its original position for machining the bearing surface. After the connecting rod was split, the end cap was bolted back on and the crankshaft bearing surface was machined. Splitting the rod first then machining the bearing surface was critical to ensure a perfectly round bearing hole. If the hole was drilled first, the hole would become non-circular due to the material that would be lost to blade thickness during the splitting process. With the bearing surfaces machined, the last step to complete the rod was to add an oil hole for lubrication. The radius in the CFRP loop in Figure 11 was chosen as the oil hole location because it mimicked the stock connecting rod's geometry. A standard drill press was used to drill the hole. Figure 12 shows the end result of the split connecting rod where the bottom part of the CFRP loop had been removed to reduce more weight. This portion of the loop no longer provided any strength because the connecting rod had been split.

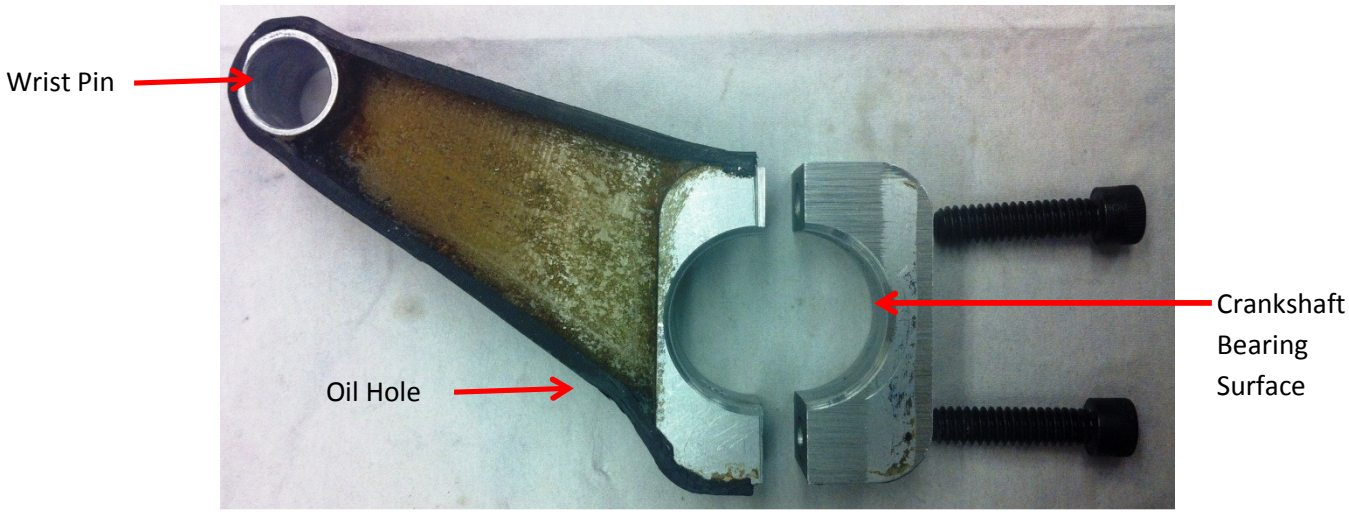

Figure 12: Split CFRP Connecting Rod

While the design of the components to withstand the forces and temperatures of the engine is imperative to a successful study, the manufacturing process was of paramount importance in this study. Composite materials provide a unique set of challenges that this study has worked to overcome and provide insight as to how to avoid pitfalls during the manufacturing stage of follow on studies.

3 Experiment and Computer Model Details

3.1 Engine Specifications

The engine used in this study is the Honda GC-160 gasoline engine. The specifications of the engine are listed in Table 1. This engine was chosen as the test platform because it is inexpensive, air-cooled (similar to UAV engines), and uses an overhead camshaft (OHC) design which facilitated the design of the crankcase. An OHC design avoids the necessity to align the camshaft as well as. Extending this study to a diesel engine would involve higher combustion pressures, and therefore more CFRP material. The weight savings would not necessarily go down, however, because the stock diesel engine would likely use more metal to handle the higher pressures, and therefore would have a greater potential for weight reduction.

Engine Type	Honda GC-160 Air-cooled 4-stroke OHC
Cylinders	1
Bore x Stroke	2.5" x 2.0" (64 mm x 50 mm)
Displacement	9.8 cu in (160 cm3)
Net Power Output	4.6 HP (3.4 kW) @ 3600 rpm
Net Torque	6.9 lb-ft (9.4 Nm) @ 2500 rpm
Compression Ratio	8.5:1
Fuel	Unleaded 86 octane or higher
Lubrication System	Splash
Dry Weight	25.4 lbs (11.5 kg)

Table 1: Honda GC-160 Engine Specifications

3.2 Instrumentation

The instrumentation employed throughout this study aimed to collect material properties, thermal data, and strain data. The material properties were collected using two tensile test apparatuses, a MTS 20kip Stand with Flex Test Control Software and an Instron/Instrumet stand with an Instron oven. A high temperature Instron extensometer was used to measure the strain in the samples through a large range of temperatures. The samples were all pulled to test ultimate strength of the material in order to calibrate Finite Element Analysis (FEA) models. These models would be used for optimization of the composite components after initial testing was completed.

In order to collect the stock engine's operating temperature, pressure trace, and strain data, the engine was tested on a Model 66 Midwest and Dynamatic Eddy Current **Dynamometer** that gives the user full control of the engine's operating speed and load point. The engine was run through its full range of speeds from maximum power at 3600 RPM to its maximum torque at 2500 RPM. Steady state operating temperatures were reached in approximately twenty minutes, at which point the temperature data was recorded. A variety of temperature measuring equipment

was used throughout the study to get the temperature of the oil, the crankcase, and the connecting rod.

Standard surface thermocouples were placed along the side of the crankcase for a temperature profile. A thermal imaging camera and a line of sight thermal gun were also used to measure the temperatures along the side of the crankcase. Figure 13 shows the image produced by the thermal camera during dynamometer testing. The oil was measured using a K-type thermocouple that was placed through the oil cap of the engine.

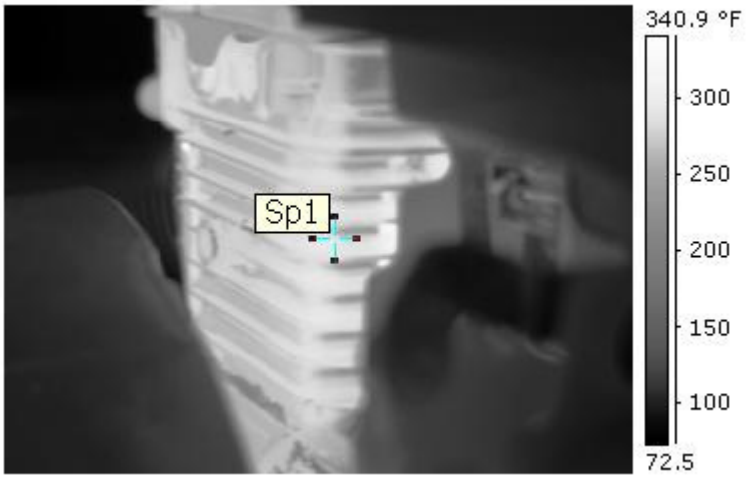

Figure 13: Thermal Imaging Camera Output

The temperature of the connecting rod proved to be difficult to measure. K-type thermocouples were wired into the surface of the connecting rod, chemically irreversible surface temperature indicators were placed on the surface, and temperature crayon indicators were tested for measuring the connecting rod temperature in situ during steady state operation. The surface temperature indicators and temperature crayon indicators were tested in a hot oil bath to ensure that they would remain intact during engine testing. The oil bath testing procedure is found in Appendix C. The crayon wiped off too easily, but the surface indicators remained attached through prolonged exposure to turbulent, hot oil during initial testing. The K-type thermocouples were epoxied into the side of the rod to ensure they stayed in place.

A Kistler Type 6117 (6117BFD17) spark plug was used to map out a pressure trace of the engine during operation at its peak torque operating point at wide-open throttle and 2500 RPM. This operating point represents the highest anticipated stresses on the crankshaft, connecting rod, and crankcase, and therefore represents the worst-case standard operating condition for these parts. As detailed in the following section, combustion was also modeled using an early combustion "knock" event that represents a true "worst-case" scenario for connecting rod stress; this "knock" event was not recreated experimentally due to concern over damage to other engine components. The spark plug transducer utilized a piezo-capacitive pressure transducer mounted in the same body as the spark plug.

Strain measurements were attempted to experimentally measure the strain on stock engine components in order to confirm modeled data and to better design a composite replacement part. In order to obtain the strain during dynamometer testing, an Omega KFG single axis strain gage was fixed at 0° and 90° and mounted below the crankshaft main bushing, as this location was hypothesized to be the location of greatest strain on the crankcase. A strain gage was also mounted on the connecting rod as shown in Figure 14. The wires were epoxied along the inside of the crankcase and run out through the oil drain hole in an attempt to measure strain on the connecting rod during engine operation. While this approach would give an accurate measurement as to what the CFRP design would need to withstand during engine operation, its success depended upon designing a wire path that would withstand the rapid motion of the connecting rod inside the engine, exposed to constant "sloshing" through the elevated oil bath The strain gages used an Omega BCM-1 full Wheatstone bridge configuration connected to an Omega DMD-465WB high bandwidth instrumentation amplifier with amplification to 2 kHz (-3 dB point). The high bandwidth is unique among strain gage amplifiers, and would allow the dynamic strain signal from engine operation (cycle frequency at 3400 rpm is approximately 30 Hz), but still provide filtering for higher frequency noise created by the spark or surrounding electronic equipment.

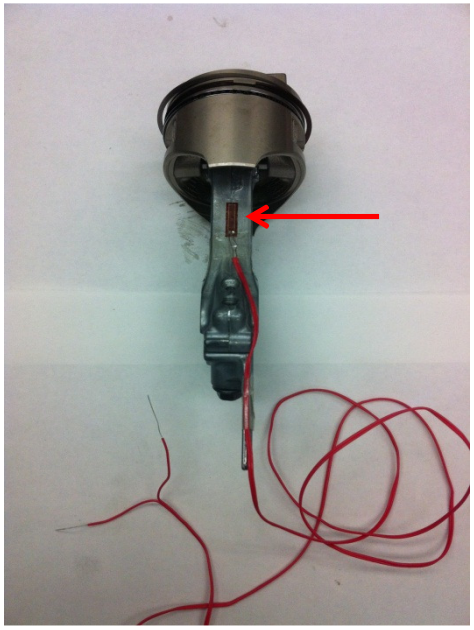

Figure 14: Mounted Strain Gage (Arrow) on the Stock Connecting Rod

Strain data was collected using a National Instruments data acquisition system using a PCI-6259 16 bit multichannel analog-to-digital converter card with a BNC-2110 breakout connector block. Temperature data was recorded using a National Instruments SCXI-1000 and SCXI-1102 thermocouple module. This data acquisition hardware was operated with National Instruments LabView software, version 8.6, collecting strain data at 1 kHz and temperature data at 1 Hz.

3.3 Computer Modeling of Engine Stresses

3.3.1 Ricardo WAVE and Reduction of Data using Microsoft Excel

Ricardo WAVE is a simulation program designed to analyze the dynamic, compressible flow of gases through an engine. The program allows the user to input combustion parameters so that it can reproduce the complete operation of an engine, giving outputs that include heat transfer rates, pressures, and temperature profiles for a given operating condition. WAVE relies completely on user input information ranging from geometries of the engine (i.e. carburetor throat diameter, intake area etc.) to combustion time and **50% burn point**, the point at which 50% of the mass of fuel has reacted with air. A 50% burn point varies with operating condition, so this study utilized a range of values with the intent to design for the worst case but to also be able to simulate actual running conditions. The 50% burn point at 0 Crank Angle Degrees (CAD) after top center (ATC) represents a very early combustion event, which could be taken to be similar to a "knock" event, a true explosion of the air-fuel mixture, which can cause great damage to the internal components of the engine if prolonged. This point represents a worst case condition for in-cylinder pressures, and therefore, worst case forces on the CFRP components. The 50% burn points of 10 CAD and 18 CAD were modeled in WAVE to represent more typical engine conditions.

Figure 15 represents the model of the Honda GC-160 that Ricardo WAVE used to analyze conditions that the engine would experience during operation. By using WAVE to model both a knock event and more typical engine operating conditions, the design of the connecting rod and the crankcase could be robust enough to survive in a worst case condition. Also, WAVE can give outputs for cases in between normal operation and knock so that designs can be tuned for weight savings versus surviving unlikely worst case operation. The models were to be validated using data collected during the dynamometer testing period. Validating the models proves the output as reliable for use during the optimization of the original component designs.

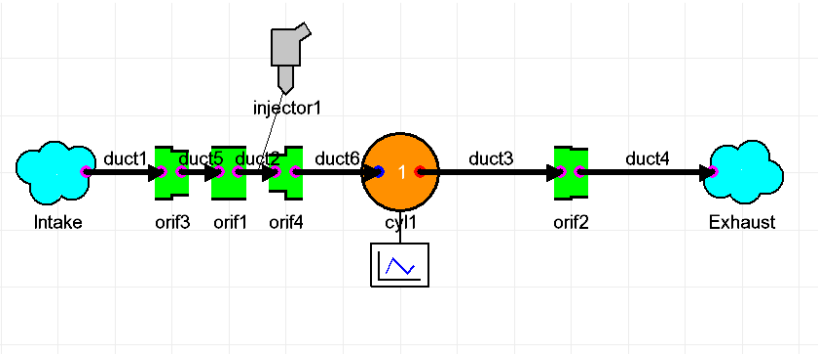

Figure 15: Ricardo WAVE Model

Figure 16 shows the output of the Ricardo WAVE model (dashed and dotted lines) compared with experimental data from actual engine operation (solid line). The 50% burn point at 18 CAD ATC (dotted line) gives the lowest predicted peak combustion pressures, but very closely resembles actual engine operation, showing excellent agreement with the WAVE model. This operating point at 2500 RPM is the maximum torque operating point of the engine and was

therefore chosen as the main operating point since maximum stresses would result at this point. The early combustion case (dashed line, knock event) shows much higher pressures, and therefore will result in significantly higher stresses on all engine components. This true worst-case scenario was also used to check final designs of composite components to ensure survivability even in this most extreme of conditions.

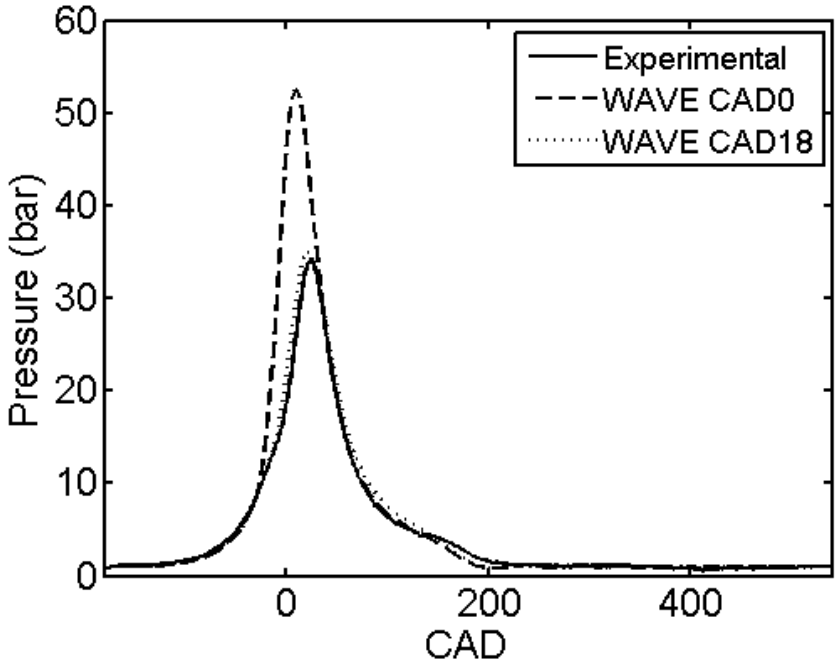

Figure 16: Ricardo WAVE Modeled Pressures at Varying 50% Burn Points, Respectively for 0CAD ATC, 10CAD ATC, and 18CAD ATC

Ricardo WAVE provides predicted temperatures and heat transfer rates of the exhaust gases. This is an essential element to designing composite components to replace the stock aluminum components. Due to the fact that composites must be brought to elevated temperatures to cure the polymer matrix, understanding the temperatures which the composite components experience is critical. The combustion gases will not directly touch the composite components in this study; however, the combustion gas temperature serves as a starting point for the heat transfer model that will predict temperatures on composite replacement components.

Figure 17 shows that Ricardo WAVE predicts that the combustion gas temperatures remain constant throughout the range of 50% Burn Points. This allows for the first node of heat transfer models to be determined, providing a more reliable model for use during the design process. Although the combustion gas temperatures are independent of 50% burn point, the heat transfer rate is not.

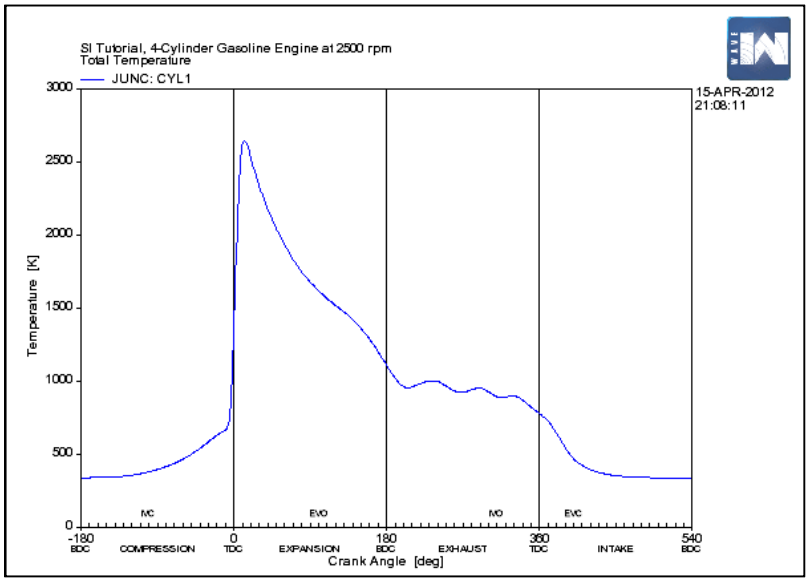

Figure 17: Ricardo WAVE Modeled Combustion Gas Temperatures

The heat transfer rate impacts the design process because the higher heat transfer rates will result in increased temperatures along the side of the combustion chamber down to the base of the engine. These higher temperatures must be mitigated by either increasing the cure temperature of the epoxy used for the CFRP or by redesigning fewer of the components with CFRP. Reducing the amount of CFRP in the redesign process, by only replacing the lower half of the crankcase for instance, the operating temperatures will have lowered by the time the energy travels down the crankcase to the CFRP portion. Additionally, less CFRP provides a larger heat sink for the combustion gas energy because the more conductive aluminum will take the energy and transfer it to the air via convection. Figure 18 shows that as the 50% burn point is advanced, the heat transfer rate decreases. At 0CAD ATC, the maximum instantaneous heat transfer rate predicted is approximately 46 kW, while at 18CAD the maximum heat transfer rate is 32.5kW. This 30% reduction in heat transfer rates during a knock event to normal operation indicates lower operation temperatures along the side of the crankcase. The WAVE analysis of heat transfer rates is imperative to formulating an accurate heat transfer model. By finding the mean heat transfer rate predicted, along with the defined node temperature from the combustion gases, a heat transfer circuit can be formed. In addition to the WAVE analysis, which predicts the instantaneous heat transfer rate throughout the cycle, the overall net heat transfer rate, $\dot{Q}$, can be predicted using the **1/3 Rule**, approximating the engine thermal losses as one-third of the incoming fuel chemical energy, which is a reasonable, first-order approximation for most reciprocating piston engines.

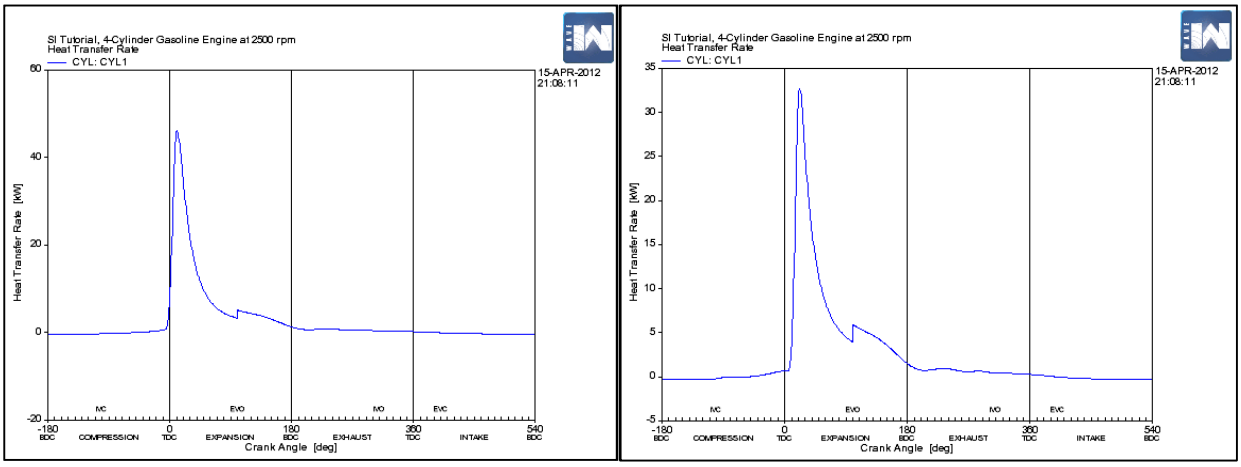

Figure 18: Ricardo WAVE Modeled Heat Transfer Rate for 50% Burn Points of 0CAD ATC and 18CAD ATC respectively

Microsoft Excel was used to reduce all data outputs and to display the results in figures.

3.3.2 Engineering Equation Solver

Engineering Equation Solver, EES, was used to create a **heat transfer model** that predicts the temperature at numerous nodes starting at the head of the engine down to the base of the engine. The range of nodes from the top of the engine to the base is necessary because replacing the aluminum crankcase with CFRP not only requires that the new crankcase survive the temperatures at the lower half of the engine, but also the increased thermal resistance of the CFRP must not raise the temperature of the head and cylinder walls to a level that would cause knock. The WAVE analysis already has proven that knock must be avoided to prevent stresses in the components from increasing. Furthermore, knock is undesirable from an engine durability stance regardless of what material is being used for the connecting rod and crankcase. The temperature at the junction from aluminum to CFRP is of particular importance because this point provides the greatest resistance to heat transfer. The temperature profile seen during experimentation can be seen in Figure 29. The study by Buckley[3]. that analyzed the feasibility of using CFRP valves in engines found that when the fibers are perpendicular to the direction of heat transfer, it is more likely to burn a hole in the CFRP. Once the model was created using the Ricardo WAVE outputs, calculated thermal resistances, and dimensions of the engine, the model was tuned using data collected during dynamometer testing to achieve the results seen during actual run time. The heat transfer model was able to replicate the stock aluminum engine's temperature profile, but it was not able to replicate the CFRP crankcase's temperature profile. Figure 19 shows the output for the stock crankcase. The CFRP model results in divergences along the crankcase that are far too great to be realistic and are not near the recorded temperatures seen during testing. Appendix F shows the code used to model the aluminum crankcase.

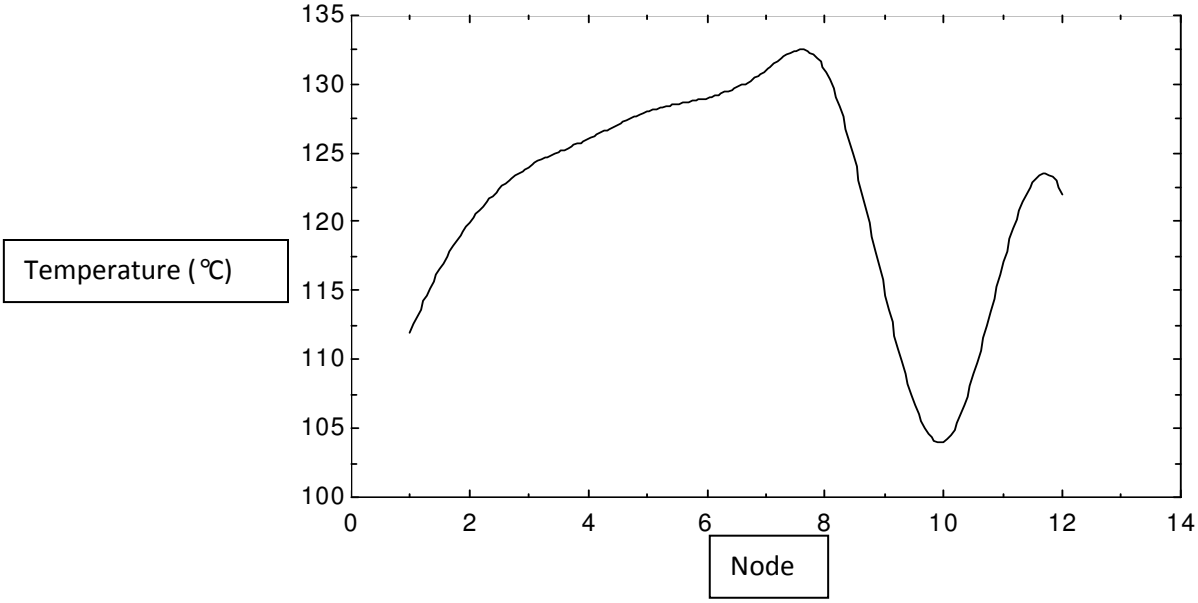

Figure 19: Engineering Equation Solver Output for Aluminum Crankcase Heat Transfer Model

3.3.3 Solid Works Finite Element Analysis

Solid Works was used to create a model of the CFRP connecting rod, as seen in Figure 20. This model allows for testing (to an extent) and optimization to be performed all in a software environment instead of by crush testing and dynamometer testing every change and iteration of the connecting rod. The software used is called Finite Element Analysis (FEA). By applying material properties to each component of the model, FEA can analyze the survivability of the part using user inputted forces.

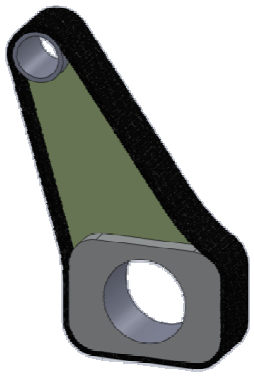

Figure 20: Solid Works Model of the CFRP Connecting Rod

The experimental load data from running the stock engine was used to apply forces to the solid works model. The material testing conducted yielded the material properties necessary to calibrate the model in order to have accurate predictions of high stress areas in the part. The combination of both tests was used in the FEA analysis of the connecting rod. Figure 21 is the output of the FEA analysis. The blue and green areas are areas of lower stress while the yellow orange and red represent high stress areas on the part. The radius of the CFRP loop near the lower crankshaft bearing experiences the highest stress because of the sharp corner created as the CFRP angles away from the coin. The FEA test conducted on the CFRP connecting rod did not predict failure of the part in compression at the peak load of 11kN.

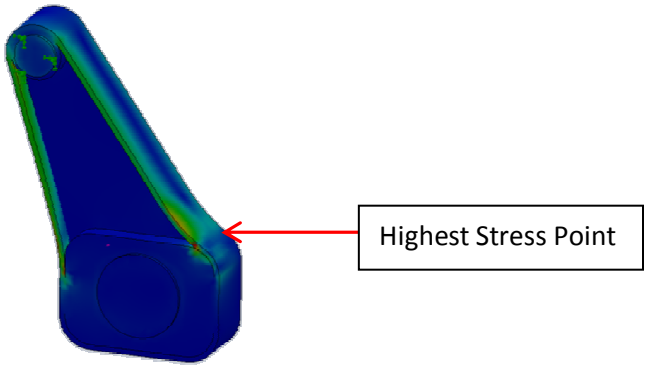

Figure 21: FEA Output for the CFRP Connecting Rod

FEA can be used to improve the design of a CFRP component once a first iteration is complete. A second iteration with less material, resulting in more weight savings, can be designed in Solid Works and tested using FEA to prevent the waste of resources caused by constant destruction of iterations in crush tests.

4 Results

Before an undertaking the size of this study began, the feasibility of the proposed research was analyzed. Basic calculations were done to ensure that switching a component from aluminum or steel to CFRP would not require a dramatic increase in component size. A CFRP cylinder was chosen to compare stresses in CFRP to metal for a given peak combustion pressure. The peak combustion pressures ranged from gasoline engines (30atm-50atm) to diesel engines (80atm-110atm) to ensure feasibility in all potential applications. Figure 22 shows the preliminary calculations' predicted wall thicknesses required to survive the loads applied by the aforementioned peak combustion pressures. These wall thicknesses, although greater than steels, are not unreasonable and prove that CFRP will not require unreasonable geometries to replace the traditional metal components.

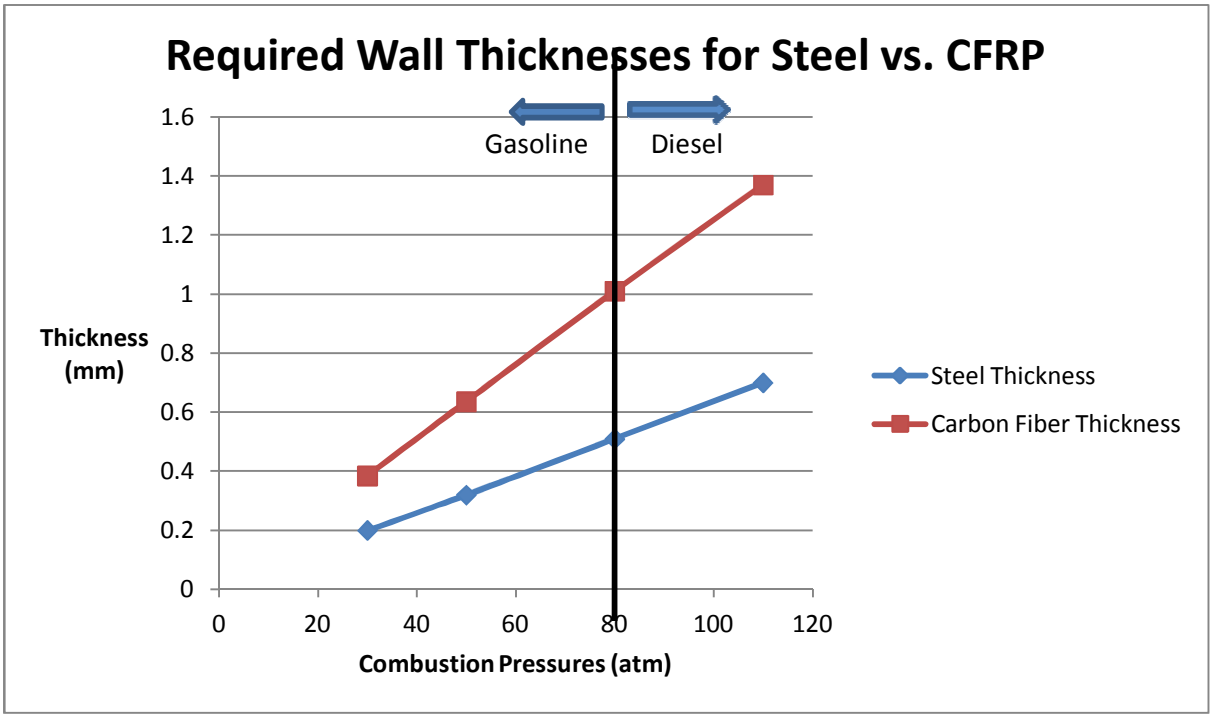

Figure 22: Preliminary Calculations' Predicted Wall Thicknesses of CFRP vs. Steel

4.1 Material Testing

In order to validate the model's predictions, accurate properties of the materials to be used were required. The elevated temperatures that the engine operated at also required evaluating what effect raised temperatures have on CFRP properties. The crankcase material was tested for each of the various orientations used throughout the different faces to ensure that the strength and stiffness was adequate to survive dynamometer testing.

Tensile tests were performed on each of the different wall orientations to determine material strength and stiffness. As the tensile test machine pulls, a data logger records the force at which the sample is being pulled and the extensometer records how much the sample stretches. With the force data and the stretch data, stress and strain can be calculated. Notice in Figure 23 that each line corresponds to a different layup orientation for different faces of the crankcase. Figure 23 shows that the flange material proved to be the strongest and the stiffest of the faces using 8 layers of 0°-90° oriented fibers. The **Modulus of Elasticity,** 59.8GPa, is comparable to the stock aluminum which is approximately 69 GPa. The comparable stiffness is significant because the flange must not bend along the length of CFRP between each bolt that holds the crankcase to the upper portion of the engine. If the stiffness is too low, the bending that results between bolts likely would break the gasket seal that maintains the crankcase pressure necessary to run the fuel pump. In our testing we did not use the pump, instead we gravity fed the fuel by hanging a fuel tank above the engine and linking it directly to the carburetor. The high strength of the flange is also necessary to withstand the forces from the bolts due to combustion. The eight bolt holes along the flange act as stress concentrators, however the ultimate tensile strength of approximately 600 MPa gives the flange a high probability of survival. The ultimate tensile strength of aluminum is 110 MPa. The sidewalls and load bearing face both have significantly higher strengths than aluminum at 465 MPa and 512 MPa respectively.

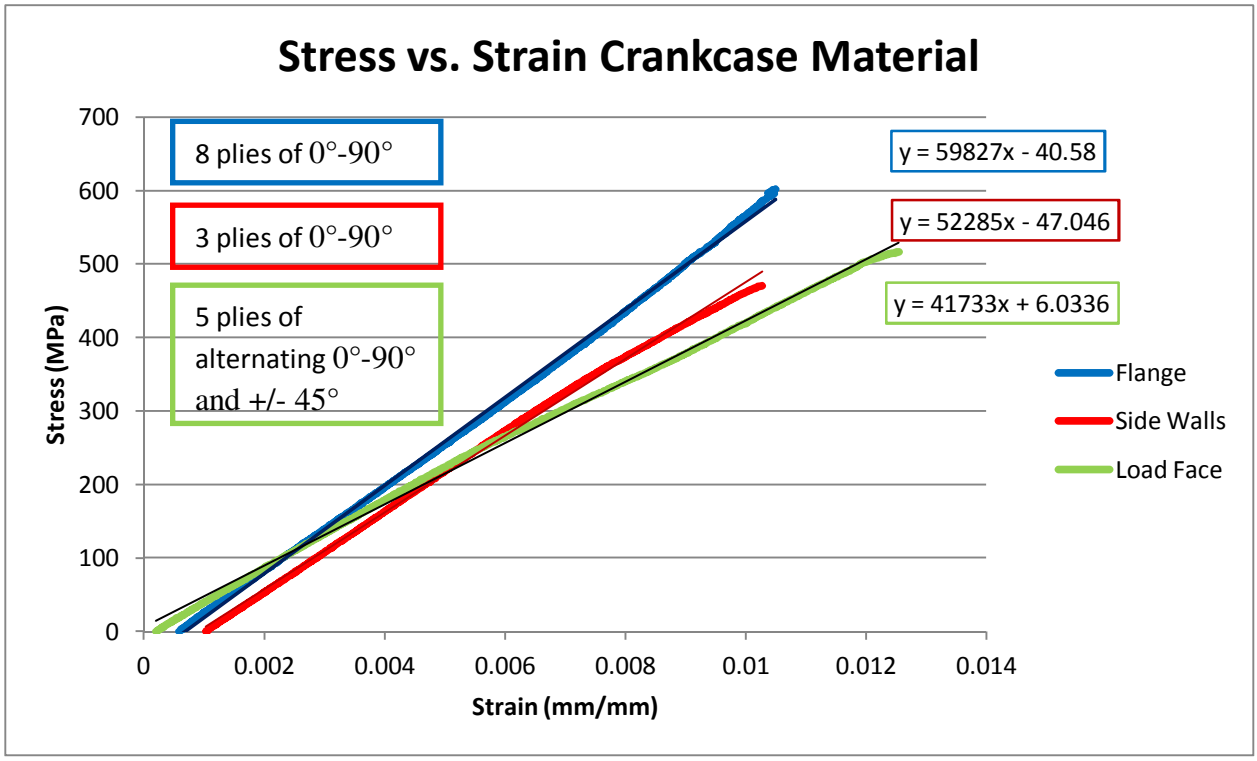

Figure 23: Stress vs. Strain for the Crankcase Material in the Flange, Side Walls, and Load Bearing Face

The connecting rod CFRP to be used was a combination of pre-impregnated unidirectional fibers with +/-45° oriented fibers. Test specimens were made for testing at various temperatures to fully understand the effect that temperature has on the strength and stiffness of CFRP. Due to

extensometer slip (no strain data, only force and head displacement), only one sample result for 60°C and one 180°C was included in the stiffness data, but the ultimate strength was still accurate.

The data in Figure 24 suggests that the stiffness of the CFRP is relatively constant throughout the range of temperatures from 25°C to 120°C. This trend is relevant because the connecting rod will clearly need to withstand the operating temperatures of approximately 140°C. Once the temperature was raised to the cure temperature, the stiffness dramatically tapers off. Figure 24 shows that in the initial stages of the 180°C test, the slope is comparable to the other temperatures' data until approximately 0.005 strain, but a failure in the matrix of the material leads to the decreased strength and stiffness. The operating temperature of the connecting rod approaches the cure temperature; however it never reaches this critical curing temperature where the polymer matrix begins to gel when the part is formed. No failure would be expected at much lower stresses.

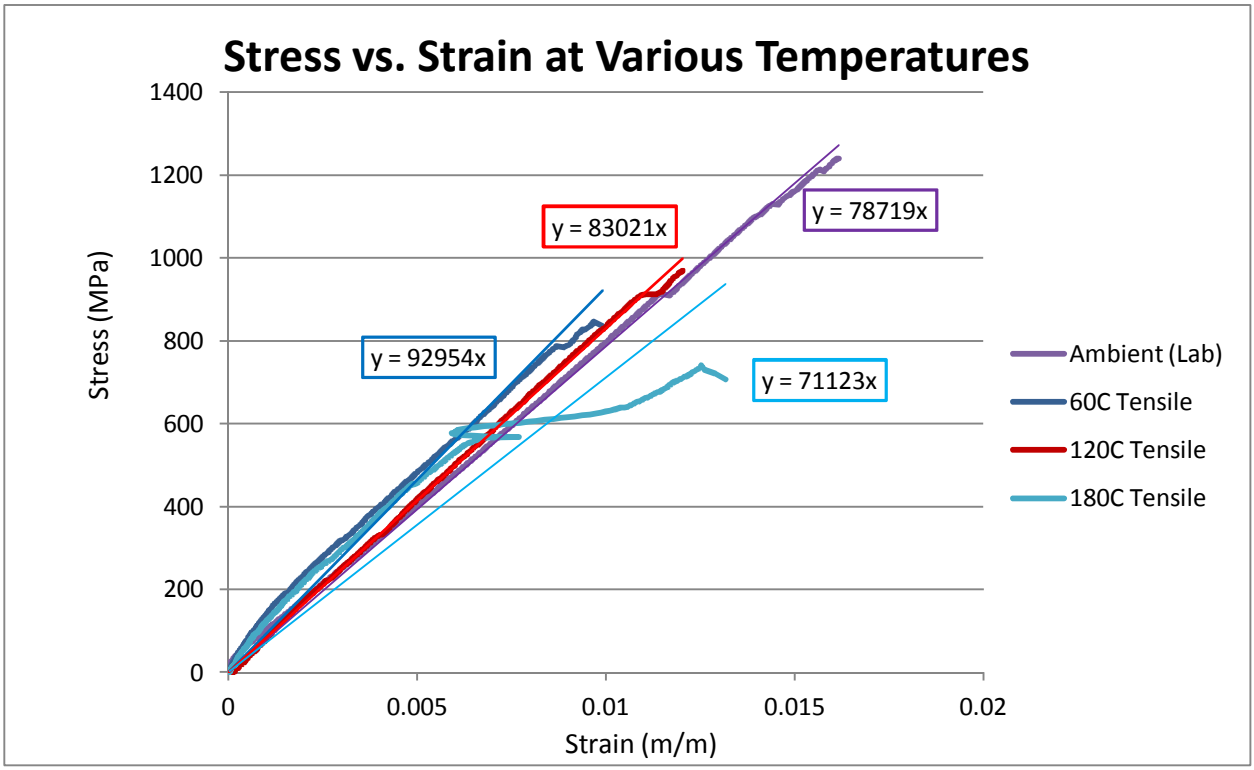

Figure 24: Stress vs. Strain for the Connecting Rod Material at Temperatures Ranging for Room Temperature (25°C) to the CFRP Cure Temperature (180°C)

The effect temperature has on the CFRP's ability to withstand loading from combustion forces is analyzed in Figure 25. Two sample results at each temperature are averaged to give each data points of Figure 25. There is a downward trend in the strength data as the temperature is elevated, but the drop from room temperature to 60°C and then the increase from 60°C to 120°C indicate that the strength variations may be due to material layup and not due to the temperature. Therefore, it is assumed that the strength of a composite material may drop slightly from room temperature to an elevated temperature but then remains constant until the curing temperature.

The operating temperature of the engine's stock connecting rod, 140°C, will not significantly alter the strength of the CFRP. As the CFRP reaches the cure temperature, the matrix holding the fibers together begins to soften. The +/-45° weave begins to move in line with the axial force being applied once the load is high enough to move the fibers through the softer matrix. The alignment of the fibers results in strain increasing at a greater rate because the fibers themselves are not being stretched, but instead are moving to align with the force, giving the part a greater length. This increased rate of strain results in a decreased stiffness. At the cure temperature of 180°C, the ultimate strength represents the strength dominated by the fibers alone. The failure observed at 180°C was delamination of the plies, specifically the +/- 45 plies from the uniaxial ply layers.

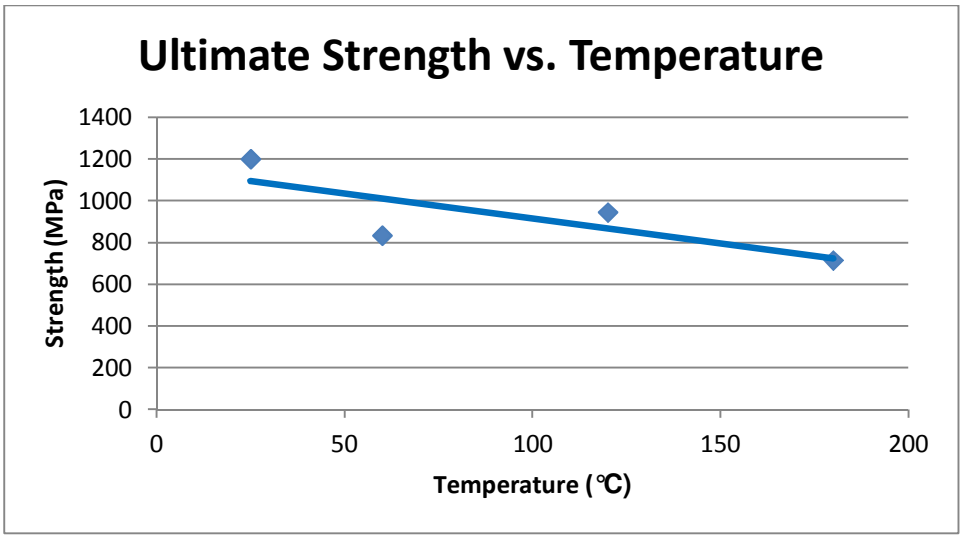

Figure 25: Ultimate Strength of the Connecting Rod CFRP at Temperatures ranging from Room Temperature to the CFRP's Cure Temperature.

The CFRP outperforms the stock aluminum parts in ultimate tensile strength at every temperature range. Table 2 documents that the lowest ultimate strength observed was 715 MPa at 180°C. This is 6.5 times greater than the ultimate strength of aluminum, even at the operating temperature of 180°C. The average ultimate strength of approximately 993 MPa across the full range of temperatures below cure temperature is 9.0 times greater than that of aluminum. The CFRP has comparable stiffness properties throughout the full range of temperatures below cure temperature as well. With an average modulus of elasticity of 84.9 GPa, the CFRP outperforms aluminum with a modulus of elasticity of 69 GPa. As seen in Table 2, bringing the CFRP to cure temperature reduces the modulus of elasticity due to failure of the matrix.

Temperature (°C)	Ultimate Strength (MPa)	Modulus of Elasticity (GPa)
25	1200	78.7
60	834	93.0
120	945	83.0
180	715	71.0
Aluminum (25°C)	110	69.0

Table 2: Tabulated Results of Material Properties vs. Temperature

The data proves CFRP to be a viable replacement material for aluminum given that the operating temperature does not equal or exceed the cure temperature. In order to prove that the designs using CFRP will also survive the worst case forces calculated by using the Ricardo WAVE analysis, the material data must be coupled with the WAVE outputs.

Using the pressure trace obtained from dynamometer testing of the stock engine and two of the pressure traces predicted by Ricardo WAVE, three connecting rod force scenarios were developed. Figure 26 shows the forces given any angle of the crankshaft for the max torque point, an ideal operating condition simulation, and a knock event simulation. The force within the connecting rod is not only important to analyze the predicted stresses in the CFRP connecting rod design, but also for the CFRP crankcase since all loads are transferred from the piston face to the engine's base through the connecting rod and down the sides of the crankcase. Given the geometry of the CFRP connecting rod and crankcase, the stresses were calculated for each condition above and compared to the results of the material tensile testing.

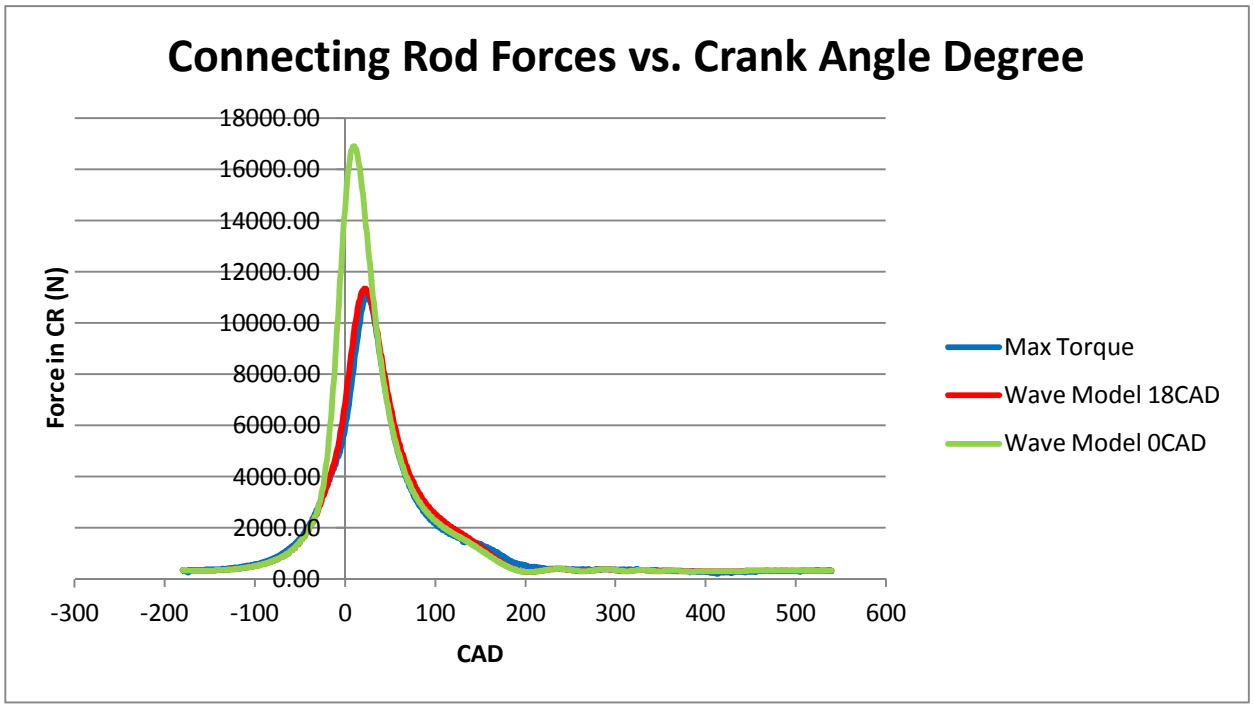

Figure 26: Forces in the Connecting Rod for Varying Operating Conditions

Both the connecting rod and the crankcase design for CFRP replacement are capable of surviving loading conditions ranging from normal operation to engine knock conditions. Given the data obtained during the tensile testing, Figure 27 shows that the crankcase has a **factor of safety**, FS**,** of 3.8 if the engine begins to knock. Knock is an unlikely event so the true FS is much greater than 3.8.

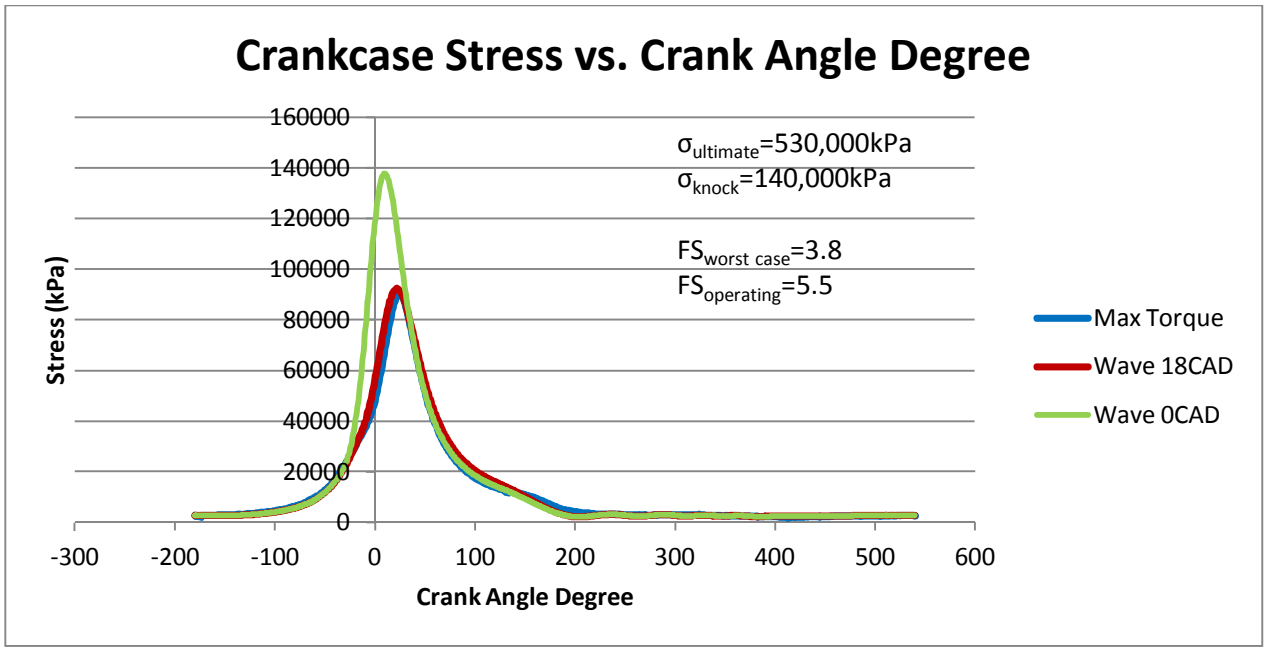

Figure 27: Stresses in the Crankcase's Load Bearing Face for Various Loading Conditions

Figure 28 shows that the FS for the connecting rod is 1.5 given the stresses achieved for the maximum load applied during testing. When testing the crush strength of the CFRP connecting rod, the apparatus' arms began to bow outwards, potentially creating conditions that could cause damage to the load cells, so the test had to be stopped before failure. Repetitive crush testing, both at room temperature and at a maximum predicted operating temperature of 160°C, showed that the coins used as bearing surfaces begin to separate from the CFRP loop. This separation transfers all of the loading from the CFRP loop to the G10 core, causing failure at approximately 25% of the maximum stress achieved during the crush test that did not experience coin separation. The graph in Figure 28 below is annotated with the connecting rod stress observed when the coins did not separate and does not represent the stress that would destroy a connecting rod with sufficient bond strength. In order to prevent separation, better coin surface preparation, a stronger epoxy, and higher cure temperature must be used to allow for survival in both fatigue and high temperature operation.

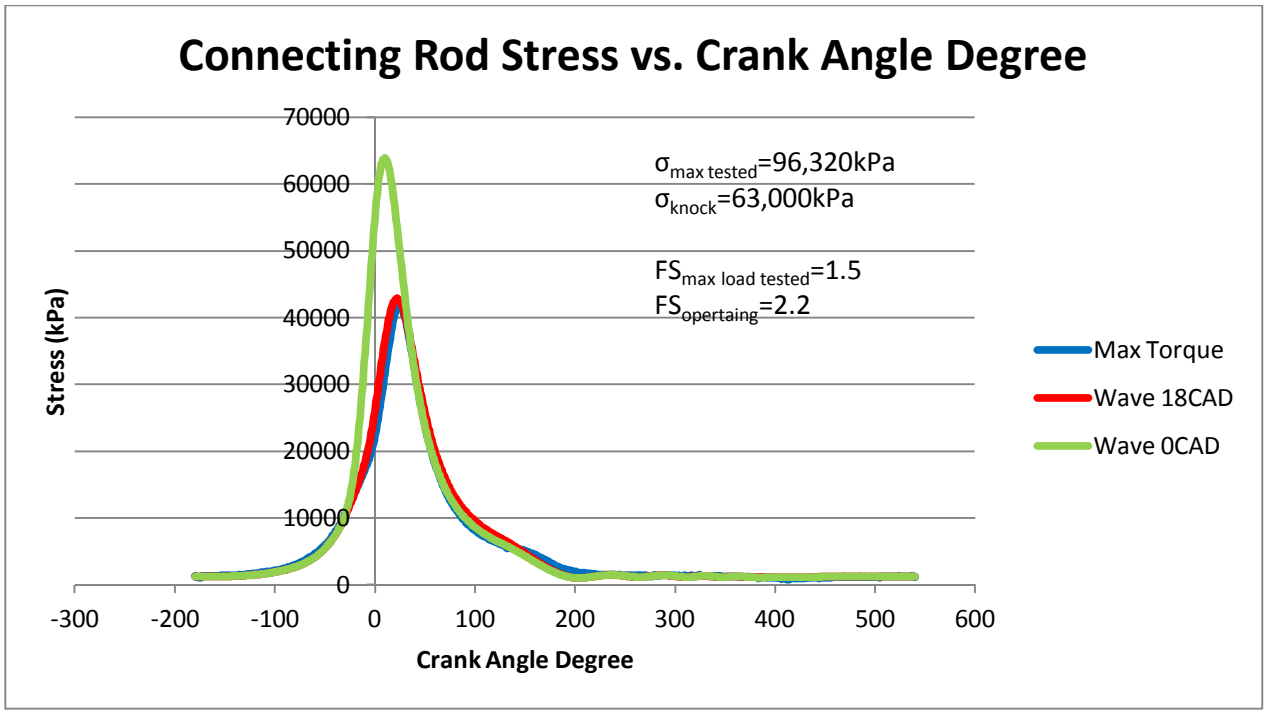

Figure 28: Stresses in the Connecting Rod for Various Loading Conditions

In both designs the CFRP components are capable of surviving loading much greater than what is anticipated. These factors of safety provide room for optimization, and further weight reductions in the engine. Of course, reducing the material used will require a trade-off between weight reduction and reliability of the components.

4.2 Initial Dynamometer Testing

To develop data to determine the likely performance of a CFRP component in the engine, the stock engine was operated on a dynamometer to collect temperature, pressure, and strain data.

The thermal imaging camera and line of sight (LOS) temperature sensor used to measure engine exterior temperature provided the node temperatures along the side of the stock crankcase. The temperatures remained below the failure temperature of the wet layup epoxy down the case. From the head to the junction of cylinder wall to the beginning of the crankcase there was a linear decrease in temperatures. At the junction, the temperature spiked due to the high resistance from the gasket material that seals the crankcase, and presents a large thermal resistance to thermal energy flow. Below the case junction, temperatures decreased linearly as expected as distance from the combustion chamber increased until the node that represents the oil height line. Figure 29 shows the temperature profile of the engine and Table 3 documents the node temperatures, showing that no temperature exceeds the epoxy's failure temperature of 180°C. The operating temperature of the oil is essentially equal to the highest steady-state operating temperature of the upper portion of the crankcase, even next to the combustion chamber.

Therefore, the oil operating temperature can be used to assess the viability of a CFRP replacement crankcase component.

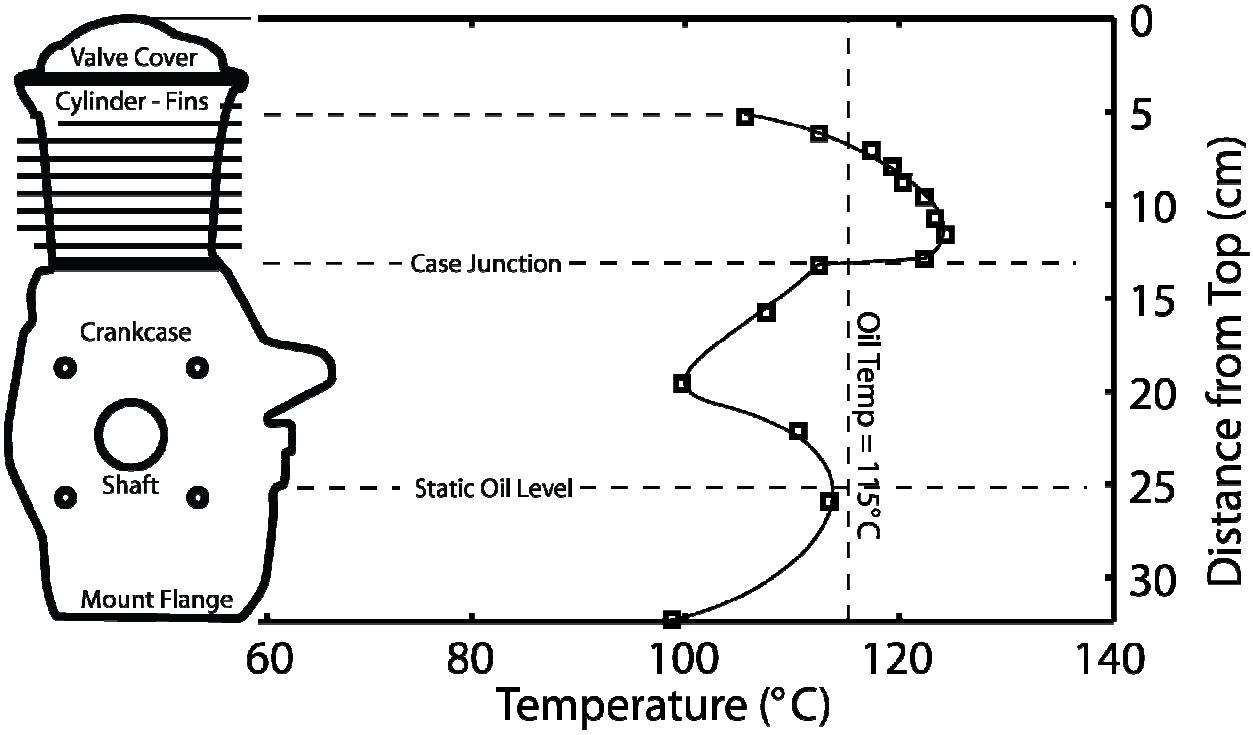

Figure 29: Diagram Displaying the Thermal Node Positions along the side of the Engine

Node	Location	Temperature (°C)
Fin Gap	1	105
Fin Gap	2	112
Fin Gap	3	117
Fin Gap	4	119
Fin Gap	5	120
Fin Gap	6	122
Fin Gap	7	123
Fin Gap	8	124
Case Junction	Top	122
Case Junction	Bottom	112
Case	1" down	107
	2.5" down	99
	3.5" down	110
	5.0" down	113
Case Base Bottom		98
Oil temperature		115

Table 3: Tabulated Results of Node Temperatures

In addition to temperature data for the crankcase, strain data was measured using strain gages mounted at a right angle in a dual-bridge configuration. This configuration reduced the effects of thermal expansion and would be necessary to design for an adequate amount of material along the load bearing face of the CFRP crankcase. Two strain gages were attached and the engine was run through all load points, from maximum speed to maximum torque, and no appreciable strain was measured in the crankcase. It has been determined that the crankcase size requirements result in an overdesigned aluminum case due to the lack of any appreciable strain. Therefore, strain in the stock crankcase was assumed to be negligible. Because the strain in the stock aluminum crank case is negligible, no strain measurements were taken on the CFRP crankcase that has similar stiffness properties of aluminum.

Temperature data for the connecting rod was obtained through the use of **irreversible chemical temperature indicators**. Wired k-type thermocouples were initially placed in small holes bored along the side of the connecting rod. The wires were epoxied down the side of the connecting rod to the side of the case in an attempt to clear the crankshaft's counter weights. This approach failed due to wire fatigue during engine operation. The epoxy created sharp radii that acted as stress concentrators, causing the wire to fail. This failure led to the choice of the chemical indicators measuring four nodes' temperatures.

The four nodes chosen in Figure 30 represent the top wrist pin, 160°C +6°C/-0°C, the first intermediate node, 143°C +6°C/-0°C, the second intermediate node, which consistently

registered temperatures higher than the indicating markers could read, and the crankshaft node, 143°C +6°C/-0°C. The indicators gave temperature readings at 6°C intervals The intermediate node closest to the crankshaft continued to overwhelm the indicators during operation because hot oil from the oil ring on the piston drips down and makes contact with the indicator during operation. Although the exact temperature of this one intermediate node could not be ascertained, the steady-state operating temperatures of the remaining nodes are well below the CFRP cure temperature of 180°C which will allow for the CFRP to maintain its high strength and stiffness properties. The apparently high temperature of the second intermediate node is likely highly localized due to oil drain from the piston—if CFRP failure was observed due to excessive temperatures at this node, local reinforcement or shielding could be utilized to counteract the oil drip.

Figure 30: Irreversible Chemical Temperature Indicators Indicating Node Temperatures of the Connecting Rod during Steady State Operation

Strain data for the connecting rod was not able to be obtained during operation. Due to the high rotational speed of the engine, the strain gage wires will rapidly fail due to fatigue (repetitive straining due to reciprocal motion of the engine). Despite great care to minimize fatigue in an attempt to at least briefly capture strain data from the connecting rod, the wire of the strain gage failed to survive engine operating conditions, as shown in Figure 31. The epoxy used to secure the wire to the inside of the case created stress concentrators that led to the rapid failure of the wire after only a few seconds, perhaps even as the engine was beginning to start firing. Given the similar modulus of elasticity values for aluminum and CFRP, and given the superior strength of CFRP compared to aluminum, a similar cross-sectional area was maintained for the first iteration of the connecting rod design to mitigate whatever strain may exist during operation.

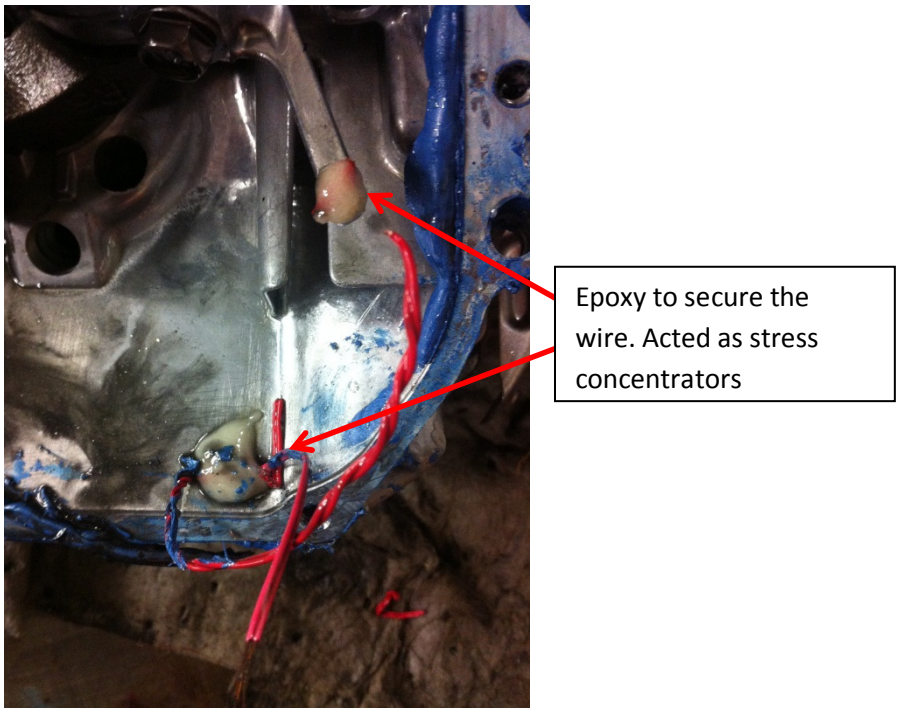

Figure 31: Failed Strain Gage Wires for Strain Measurements on the Connecting Rod

4.4 CFRP Component Dynamometer Testing

With the stock engine operating temperatures recorded, the models used for design validated by the stock engine values, and the material for use in the CFRP components tested for strength at temperature, the CFRP components were mounted on the engine for testing on the dynamometer. It was expected that these initial prototypes would fail after relatively short operation—important to the scope of this study is to understand why failure occurs. The purpose of the operational test is to provide a means to refine follow-on designs. If the CFRP part fails due to one of the predicted modes that was modeled and accounted for in the design phase, then this points to an error in design that needs to be revisited. However, if failure occurs due to an unexpected or a yet modeled mode, this points to the need for additional design work to accommodate the overlooked problem. Either result is an opportunity for improved follow-on design and important lessons learned.

The CFRP crankcase survived for twenty minutes of dynamometer testing at the maximum torque operating condition. There were two significant failure modes. First, the epoxy that secured the fiberglass base to the CFRP crankcase, to maintain stock engine height and alignment, cracked as shown in Figure 32. This crack caused excessive vibrations in the engine which resulted in the bolts securing the flange of the CFRP to the upper portion of the engine to loosen and back out; possibly due to the fact that the crankcase bolts do not use washers. Once the bolts were loosened, the engine continued to vibrate and a crack propagated along the base of the crankcase between the case and the baseplate The second failure was at one corner of the CFRP crankcase itself, where the carbon fiber had been laid on the mold with very high curvature. This curvature caused the fiber filaments to separate and created a significant

weakness in the case at the corner. This weakness could have been easily detected by physically probing this area, but it was undetected with visual observation. The failure of the case-base junction caused excessive vibration; the loosening crankcase bolts and weakened corner created oil leaks. While the engine continued to operate, the test was terminated at approximately 20 minutes due to the severe loss of oil.

This test also revealed several successful elements of the design and served to foster important lessons for follow-on work. First, the CFRP is able to withstand the loading and the temperatures of the engine operating at the max torque point (extreme operating point) for extended periods of time (prior to the excessive vibration). This was the main design criteria for the crankcase, and the experiment supported the validity of the design. Second, a proper base mounting method must be designed to support the CFRP crankcase, which allows the correct height and alignment. Third, the small hole at the corner of the case was likely due to fibers in the weave spreading over an edge during layup. This can be mitigated by taking greater care to ensure every layer of the weave is placed properly or by reducing the radius of curvature of the mold.

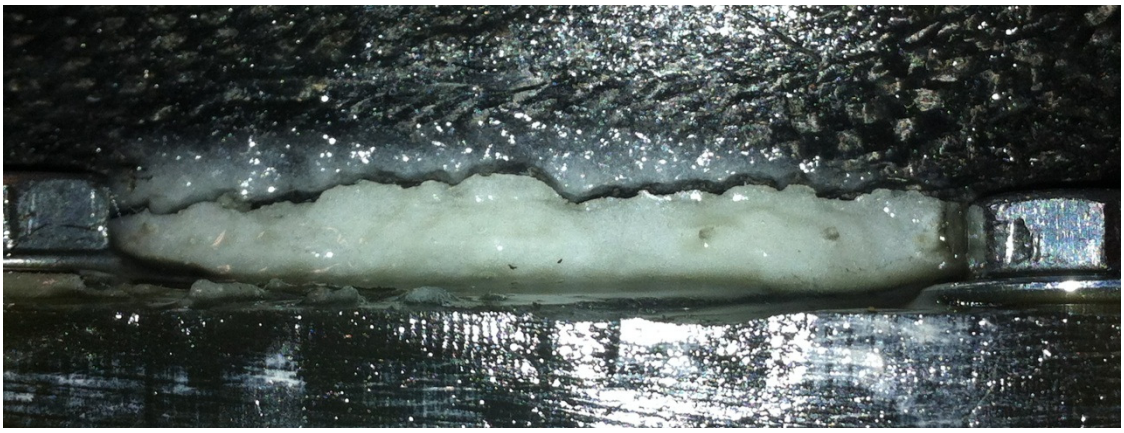

Figure 32: Cracked Epoxy Securing the Fiberglass Base to the CFRP Crankcase

The CFRP tended to run at temperatures that were lower than that of the stock aluminum crankcase as seen in Table 4. The **thermal conductivity** for CFRP is lower than the thermal conductivity for aluminum, especially when the plane of the fibers is perpendicular to the direction of heat transfer. This allows less of the combustion gas energy to dissipate into the CFRP crankcase, keeping the temperature lower. The significance of lower temperatures in the CFRP is that the material will maintain its strength and stiffness while there is a larger buffer between operating temperature and cure temperature.

Location on the Crankcase	CFRP Case Temperature (°C)	Stock Case Temperature (°C)
1" down	95	107
2.5" down	76	99
3.5" down	87	110
5.0" down	86	113

Table 4: Temperature Profile of the CFRP Case at Steady State

The CFRP connecting rod was tested on the dynamometer as well. Once the engine was started, the dynamometer held the speed at 3700 RPM for approximately 30-60 seconds. Then the engine was brought down at 100 RPM increments until the maximum torque point was reached. At the beginning of the test, a strange ticking sound was heard coming from the crankcase. 130 seconds into the test, the connecting rod failed, bringing the engine to a stop.

Figure 33 shows what likely caused the ticking sound from within the crankcase. The connecting rod had made contact with the bottom of the cylinder wall, due to being just slightly oversized, creating a small notch in the aluminum. The connecting rod lasted for 130 seconds so the contact was likely not the cause of the failure. In fact, the connecting rod was likely strong enough to actually carve out this notch in the aluminum.

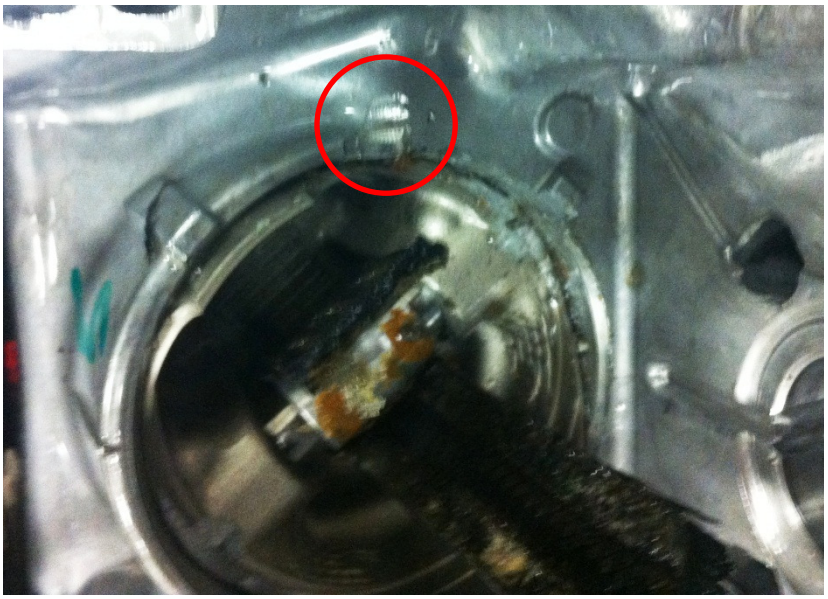

Figure 33: Contact Point of the Connecting Rod and the Cylinder Wall

The connecting rod pieces were inspected to further investigate the cause of failure. When the crankshaft was rotated, it was noticed that the lower coin used as a bearing surface would not spin freely any longer. The bearing surface had seized on the shaft, shown in Figure 34, and required significantly more effort to remove than it took to install.

Figure 34: Seized Bearing Surface

The bearing surface seizing is what is believed to be the cause of failure. The momentum of the engine caused the crankshaft to continue to spin while the bearing surface seized, causing the coin to freeze in position. Poor lubrication or thermal expansion may have caused the bearing to seize. The momentum broke the bond between the aluminum coin, the CFRP loop, and the G10 core. Once the aluminum coin was no longer attached, the piston was not able to continue to move up and down the cylinder, leaving the remaining parts of the connecting rod dangled in the path of the spinning crankshaft. This caused more damage and resulted in what looked like the catastrophic failure in Figure 35. The likely cause of this failure was improper sizing of the main connecting rod-to-crankshaft bearing, resulting in limited lubrication. The bearing must maintain an adequate gap to allow an oil film to persist; without this lubrication, excessive friction can cause the joint to stop rotation. This “failure” represents a mundane manufacturing mistake—improper sizing of the bearing. While this is an important lesson learned, the test failed to uncover a failure mode directly associated with the CFRP composite connecting rod, or to uncover the potential viability of the design. Over the course of this 130 second test, the connecting rod likely did not fail due to any failure of the CFRP or integration of CFRP with the G10 and aluminum bearings.

Figure 35: Catastrophic Failure of the CFRP Connecting Rod

Figure 35 shows that the CFRP loop itself did not fail, rather that the parts within the CFRP loop were torn out.

4.5 Weight Savings

Weight savings were analyzed, as seen in Table 5, for evaluating the utility in switching to CFRP. The CFRP case without the bushing from the stock case weighed 186 grams. The weight of the stock case with the bushing cut out was 1091.5 grams. The CFRP crankcase successfully reduced the component's weight by 83% and the overall engine's weight by 7.9%. The bushing was not used in the weight calculations because the bushing had unnecessary geometry aside from the lubrication holes that were not removed due to time constraints. Using the stock case without the bushing and the CFRP case maintained the fair comparison of weights. The aluminum connecting rod weighed 99.5 grams while the CFRP connecting rod only weighed 73.5 grams, reducing the weight of the component by 26.1% and reducing the weight of the engine by 0.2%. The total weight reduction achieved by replacing the connecting rod and the crankcase with CFRP is 8.1%, theoretically increasing the range of a UAV by approximately the same extent.

Part	CFRP Weight	Aluminum Weight	Savings
Crankcase	186 grams	1091.5 grams	83.0%
Connecting Rod	73.5 grams	99.5 grams	26.1%
Engine			**8.1%**

Table 5: Component Weight Savings

5 Conclusions and Lessons Learned

The following conclusions concerning CFRP components replacing standard metal components can be made:

1. A composite connecting rod and crankcase have material properties that allow for the implementation into UAV engines as replacement parts for standard aluminum or steel components.
2. Weight savings through the use of CFRP can be achieved. Expected weight savings by replacing a crankcase and connecting rod can be 80% and 20% respectively. Greater weight savings can be achieved by lowering the factor of safety of each component. An overall weight savings for an engine with CFRP can be expected to be approximately 8%.
3. Commercial data on aircraft weight dependent ranges shows that a 1:1 ratio of weight savings to range improvement can be expected. This preliminary design implies an improvement in aircraft range of 8%.
4. Much greater weight savings can be achieved through more iterations on the designs, and through replacement of more metal components (e.g. more of the crankcase, the crankshaft, etc.)
5. Stresses due to thermal expansion can be mitigated by curing hybrid components, such as CFRP, Aluminum, and G10, at temperatures slightly lower than the CFRP cure temperature.
6. Strain on a standard crankcase is difficult to measure, if not impossible, due to the fact that the geometry of a crankcase requires an overdesigned part given the stresses that the crankcase experiences during operation.
7. A tuned thermal model can accurately model a standard engine; however, more work is required to model the temperature of an engine with CFRP components.
8. First generation prototype CFRP designs lasted for 10^3 or 10^4 engine cycles proving CFRP's strength and ability to withstand the same forces that aluminum parts withstand. Failure of each part was due to manufacturing errors that can easily be mitigated on a second iteration of each part.

This study gave insight to many aspects of CFRP components in air-cooled reciprocating engines. Based on the manufacturing and testing methods described, the following lessons learned can be utilized for any follow-on work:

Carbon Fiber Reinforced Plastics should be manufactured using the higher quality autoclave method. When pre-impregnated CFRP can negotiate the geometry of a part, it should be chosen instead of using a dry weave in a wet-layup method. The autoclave ensures proper fiber to resin ratios and allows for more precise geometries, such as small radii, to be achieved. The pre-impregnated CFRP is significantly thinner than a wet-layup which allows for more material in tight clearance applications, giving the part more strength.

If a wet-layup cannot be avoided, ensure the fibers of each ply remain in the proper position around corners of the mold to prevent weak spots from forming. A weak spot in the CFRP crankcase, along with a failed epoxy layer securing the base, caused the crankcase to experience difficulties.

Finite Element Analysis (FEA) can accurately predict the performance outcome of CFRP components in engines. Tensile tests at the operating temperature must be used to calibrate the materials being modeled.

CFRP does not experience any significant decrease in strength or stiffness as it is exposed to elevated temperatures. Data shows that there is a slight downward trend in ultimate strength as the temperature increases, but this trend is affected by the performance of the CFRP at the cure temperature, where the ultimate tensile strength and **Young's Modulus** drop off significantly. Failure at the cure temperature is caused by failure in the polymer matrix.

Assuming the bond between the aluminum coins and the CFRP loop is strong, the connecting rod will withstand combustion forces. High cure temperature epoxy should be used in conjunction with proper surface preparation of the coins to achieve a proper bond. If the bond is not correctly prepared or operating temperatures exceed that of the epoxy's cure temperature, the coin will become loose and transfer the combustion loading to the G10 core. This load transfer will cause failure.

Both the CFRP crankcase and the CFRP connecting rod are viable replacement options for the stock aluminum parts. The testing of each part experienced difficulties and eventual failure of the parts. However, these difficulties and failures can be attributed to the manufacturing process that introduced a weak point in the testing procedure, such as a failed makeshift base or the lack of proper lubrication causing a bearing to seize. The material properties of CFRP are comparable or better than that of aluminum, and second generation prototypes could be manufactured to avoid the pitfalls experienced in the first generation prototype using the lessons learned in this study.

Further work should include manufacturing second generation prototype parts. These second generation parts should take into account the difficulties experienced in the testing done to this point. Additionally, adaptation to a diesel application should be pursued. The U.S. Navy readily has access to heavy fuels such as diesel. Therefore, the manufacturing techniques and design considerations should be used to create CFRP replacements for a diesel engine, or at the very least should be subjected to diesel engine conditions.

6 References

[1] Beckmann, Hans-Dieter, and Hermann Oetting. "Fiber Reinforced Plastics for Lightweight Engine Parts."

[2] Buckley, Richard, Rudolf Stanglmaier, Donald Radford, and Bryan Willson. "A Prediction of Weight Reduction and Performance Improvements Attainable through the use of Fiber Reinforced Composites in I.C. Engines." SAE Technical Paper Series. (2003)

[3] Buckley, Richard, Rudolf Stanglmaier, Donald Radford, and Bryan Willson."Light-Weight Composite Valve Development for High Performance Engines." *SAE Technical Paper Series*. (2006)

[4] Gunyaev, G., and S. Borovskaya. "Using CFRP for the Design of a Connecting Rod for Automobile Applications." *All-Russian Research Institute of Automobile Engines*.

[5] Naval Research Laboratory, . Technology Transfer Office, n.d. Web. 16 Feb 2011. <http://www.nrl.navy.mil/techtransfer>.

[6] Kuch, Ingo, and Peter Kummerlen. "Potential for Lightweight Design of a Hybrid Connecting Rod for Automobile Applications."

[7] Szigethy, Neil. "What, A Plastic Engine!?." *Chilton's Automotice Industries*. 180.12 (1980)

Appendix A: Fuel Consumption Analysis

The motivation behind this study comes from the idea that if aircraft weight is reduced, fuel consumption will also be reduced, increasing the maximum range of the aircraft. The engines that were used to analyze power density and fuel consumption trends are indexed below in Table 6.

Number	*Engine Designation*	*Manufacturer*
Reciprocating Piston-Gasoline (Light Fuel)		
1	Lycoming IO-360-L2A	Lycoming Engines; www.lycoming.com
2	Lycoming IO-540-AB1A5	Lycoming Engines; www.lycoming.com
3	Teledyne Continental TSIO-550-C	Continental Motors, Inc.; www.genuinecontinental.aero
4	Lycoming IO-720-B	Lycoming Engines; www.lycoming.com
5	Lycoming O-235-H	Lycoming Engines; www.lycoming.com
6	Teledyne Continental IO-240-A	Continental Motors, Inc.; www.genuinecontinental.aero
7	Honda GC160	Honda Engines Group; engines.honda.com
8	Honda GX630	Honda Engines Group; engines.honda.com
9	Honda GX25	Honda Engines Group; engines.honda.com
10	Honda GX390	Honda Engines Group; engines.honda.com
11	Honda iGX440	Honda Engines Group; engines.honda.com
12	UL260i	ULPower Aero Engines; www.ulpower.com
13	UL350i	ULPower Aero Engines; www.ulpower.com
14	OS 104RX (2 stroke)	OS Engines; www.osengines.com
15	RCV91-CD (4 stroke)	RCV Engines Limited; rcvengines.com
16	RCV90-SP	RCV Engines Limited; rcvengines.com
17	OS 160FX (2 stroke)	OS Engines; www.osengines.com
18	OS 75AX (2 stroke)	OS Engines; www.osengines.com
19	Rotax 914 UL/F	Rotax Aircraft Engines; www.rotax-aircraft-engines.com
Gas Turbine (Turboprop/shaft)		
20	GE CT7-2	GE; www.geaviation.com/engines
21	GE CT7-9C3	GE; www.geaviation.com/engines
22	GE M601	GE; www.geaviation.com/engines
23	GE H80	GE; www.geaviation.com/engines
24	GE LM2500+G4	GE; www.geaviation.com/engines
25	GE LM2500	GE; www.geaviation.com/engines
26	GE LM6000	GE; www.geaviation.com/engines
27	AMT Mercury HP	Advanced MicroTurbines; www.amtjets.com
28	AMT Titan	Advanced MicroTurbines; www.amtjets.com
29	AMT Pegasus	Advanced MicroTurbines; www.amtjets.com
30	Wren 44 Gold	Wren Turbines, Ltd.; www.wrenturbines.co.uk
31	Wren 160 K Pro	Wren Turbines, Ltd.; www.wrenturbines.co.uk

32	Wren 44 Turboprop	Wren Turbines, Ltd.; www.wrenturbines.co.uk
33	GE F404-400	GE; www.geaviation.com/engines
34	GE 90-94B	GE; www.geaviation.com/engines
35	GE CF34-3	GE; www.geaviation.com/engines
36	GE CF700	GE; www.geaviation.com/engines
Reciprocating Piston-Diesel (Heavy Fuel)		
37	Cosworth Heavy Fuel UAV	Cosworth; americas.cosworth.com
38	Yanmar L48V	Yanmar; www.yanmar.co.jp
39	Yanmar L70V	Yanmar; www.yanmar.co.jp
40	Yanmar L100V	Yanmar; www.yanmar.co.jp
41	Lombardini 15LD225	Lombardini/Kohler; www.lombardinigroup.it
42	Lombardini 15LD440	Lombardini/Kohler; www.lombardinigroup.it
43	Lombardini 25LD425	Lombardini/Kohler; www.lombardinigroup.it
44	Lombardini 11LD626	Lombardini/Kohler; www.lombardinigroup.it

Table 6: Index of Engines from Figure 1

The range of an aircraft decreases with increased payload because the engine must work harder to generate the required thrust to produce the required lift, thereby using more fuel, and reducing range. Reducing the weight of an engine, while maintaining its power output, would therefore improve range (or loitering time). For a UAV, it is likely that engine weight savings would be used to increase fuel supply at take-off, thus having the same take-off weight. However, since more of that take-off weight was in fuel, which is expended during the mission, there would be an additional benefit in range or loitering time. Thus, these estimations are conservative.

Manufacturer data for propeller-driven small aircraft gives the decrease in maximum range with increase in payload, r (nm/lbm). This factor can be normalized by maximum range and typical empty aircraft weight:

$$r^* \equiv r \cdot \left(\frac{W_{plane}}{range_{max}} \right)$$

The increase in range, $\Delta range$, for a change in aircraft engine weight, ΔW_{engine}, is:

$$\Delta range = \Delta W_{engine} \cdot r$$

Defining the percent changes in weight and range using Greek letters as follows:

$$\varepsilon \equiv percent\ change\ in\ engine\ weight \equiv \frac{\Delta W_{engine}}{W_{engine}}$$

$$\eta \equiv engine\ as\ percentage\ of\ overall\ aicraft\ weight\ \equiv \frac{W_{engine}}{W_{plane}}$$

$$\alpha \equiv percent\ change\ in\ aircraft\ weight \equiv \frac{\Delta W_{engine}}{W_{plane}} = \varepsilon \cdot \eta$$

$$\beta \equiv percent\ change\ in\ aircraft\ range \equiv \frac{\Delta range}{range_{max}}$$

Then the percent change in aircraft range due to reducing the weight of the aircraft engine is:

$$\beta = \alpha \cdot r^* = \varepsilon \cdot \eta \cdot r^*$$

To provide an indication of the extent to which a change in engine weight would increase range, we examine the ratio of β/ε. This ratio tells us the percentage by which range will increase for every percentage decrease in engine weight. A value around unity indicates that any percentage change in engine weight would be reflected in the same relative change in range (i.e. a 20% engine weight reduction would yield a 20% increase in range).

Note the similarity among the normalized parameters for popular and typical propeller-driven small commercial aircraft in Table 7 below. The data indicates essentially a one-to-one relationship between engine weight savings and range improvement. Therefore, the weight reduction of 8.1% achieved by using CFRP components indicates that an aircraft using a GC-160 engine would see its maximum range increase by 8.1%.

	r	**r***	**W_{plane} (typ, empty)**	**W_{engine}**	**η**	**β/ε**
Aircraft Model	**nm/lbm**	**-**	**lbm**	**lbm**	**%**	**-**
Skyhawk	2.34	6.28	1717	278	16.2	1.02
Corvalis TTX	2.86	5.93	2600	565	21.7	1.29
Stationair	1.53	4.71	2241	443	19.7	0.932

Table 7: The Predicted Effect of Engine Weight Reduction on an Aircraft's Maximum Range

Appendix B: Connecting Rod Kinematics

B.1 Kinematic Analysis Completed by Professor S. Graham

In order to design a connecting rod that can survive during engine operation, the forces that act on the connecting rod must be calculated. Clearly the combustion pressure exerts a force onto the piston which in turn acts along the connecting rod. However, the question of whether the connecting rod experiences any bending forces, and are those forces significant, must be answered as well. To do that, a kinematic analysis was performed by Professor Stephen M. Graham, and the results of that analysis follow.

The diagram of the piston, P, connected via the connecting rod, L, to the crankshaft, C, is show below in Figure 36. Using engine speeds and the relative motion of the piston in relation to the crankshaft, the movement of each part can be calculated. With the relative motion of each part in the diagram calculated, the angular acceleration of the connecting rod is used to calculate the acceleration of the piston.

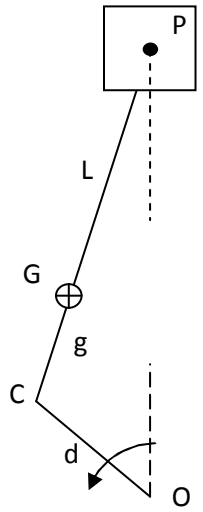

Figure 36: Diagram of the Connecting Rod

The center of gravity of the connecting rod, G, is then used to calculate its position, velocity, and acceleration relative to the crankshaft. With the acceleration of the center of gravity calculated and the pressure trace throughout a combustion cycle known from experimental data, the magnitude of the bending force can be calculated. MATLAB was used to analyze the cycle and determine the acceleration of the center of gravity throughout the fuel combustion cycle. The MATLAB output is shown in Figure 37.

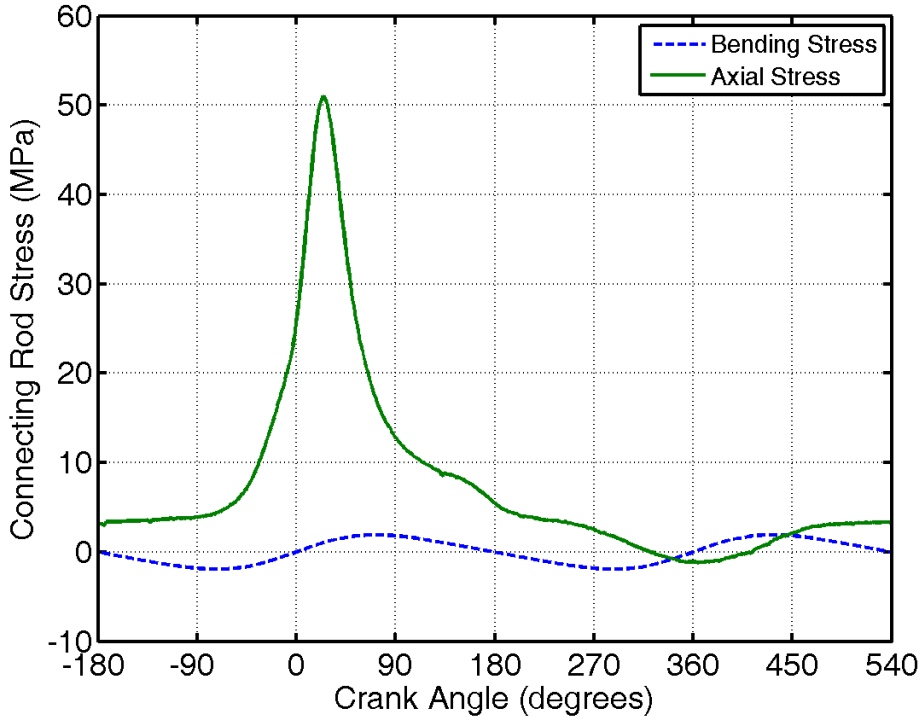

Figure 37: MATLAB Predicted Stresses

The maximum acceleration throughout the engine cycle is $1x10^5$ in/s^2, or 2540 m/s^2 and with a stock connecting rod mass above the crankshaft of .072 kg, the maximum force due to bending is 182.9 N. This bending force occurs as the piston rocks back and forth due to inertia. As seen in Figure 37, the axial stress and combustion is approximately 50MPa while the bending stress never exceeds approximately 2MPa. The bending force can be considered negligible and the connecting rod can be designed as if it were a two force member, pinned on both ends.

Appendix C: Oil Bath Testing

The initial attempts to measure connecting rod temperature and strain data during engine operation had failed due to wire fatigue. To capture the temperature during engine operation, two alternative methods were pursued. The first involved using temperature indicating crayons. These crayons worked by drawing a line on the part to be tested. The wax would change from clear to a bright color once the temperature of the part reached the temperature that the crayon was designed to indicate. The second method pursued involved sticking surface temperature indicators down the length of the connecting rod as seen in Figure 38. These indicators have four white dots and each dot represents a temperature that is 6° apart from the other dots. Once the temperature indicated is reached, the white turns to black and the change is chemically irreversible. This would allow us to place the indicators, complete the engine test, and then open the engine back up to view the temperature that each node reached.

Figure 38: Surface Temperature Indicators along the Length of the Connecting Rod

In order to determine the feasibility of these methods before committing time to an engine test, a hot oil bath test was conducted to ensure that each method would survive the hot oil environment. The oil bath test setup can be seen in Figure 39 where a hot plate was used to heat the oil to operating temperatures. A magnetic wand was used in conjunction with the hot plate to continuously move the oil to simulate oil splashing onto the connecting rod.

Figure 39: Hot Oil Bath Test Setup

The temperature crayons were drawn onto an aluminum piece to be swirled in the oil. This tested the crayon's resistance to washing off in the oil. When the lines were drawn on the oil, it was difficult to get a consistent and noticeable line to stick before the test. The crayon that was on the aluminum did not survive the hot oil bath. It washed off or ran down the aluminum, indicated that any chance of working correctly within the engine was small.

The surface temperature indicators were tested in a manner consistent with that of the temperature crayons test. The aluminum was covered with a range of temperature indicators for temperatures from 99°C to 188°C. This range was used to ensure that the lower temperature ranges would survive the higher temperatures of the splashing oil. This also tested the effect that the oil had on the unchanged dots of the higher ranges so that no false readings were recorded. When the aluminum stick was submerged in the hot oil bath for an extended period of time, there was no sign of the indicators falling off. In fact, when the test was complete considerable force had to be used to scrape the indicators from the aluminum. The method selected for testing the connecting rod during engine operation was the surface temperature indicator.

Appendix D: Photographic Documentation

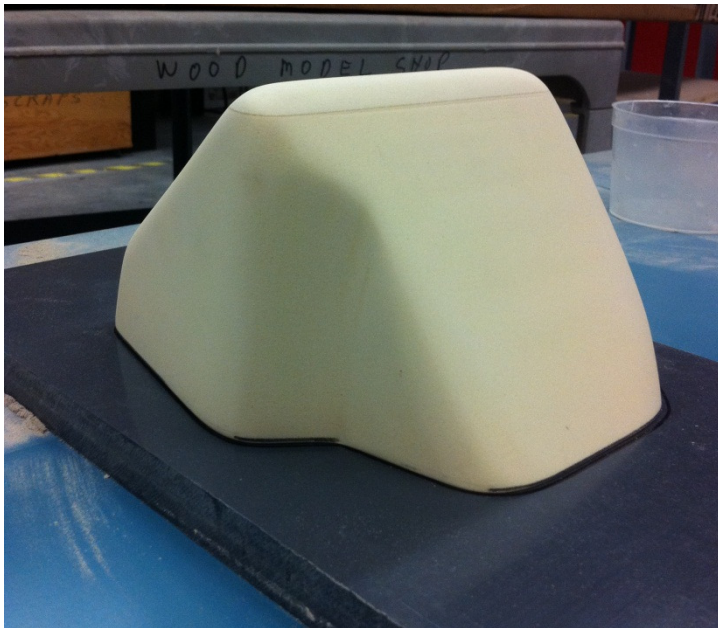

Figure 40: Crankcase Mold Mounted Prior to Priming

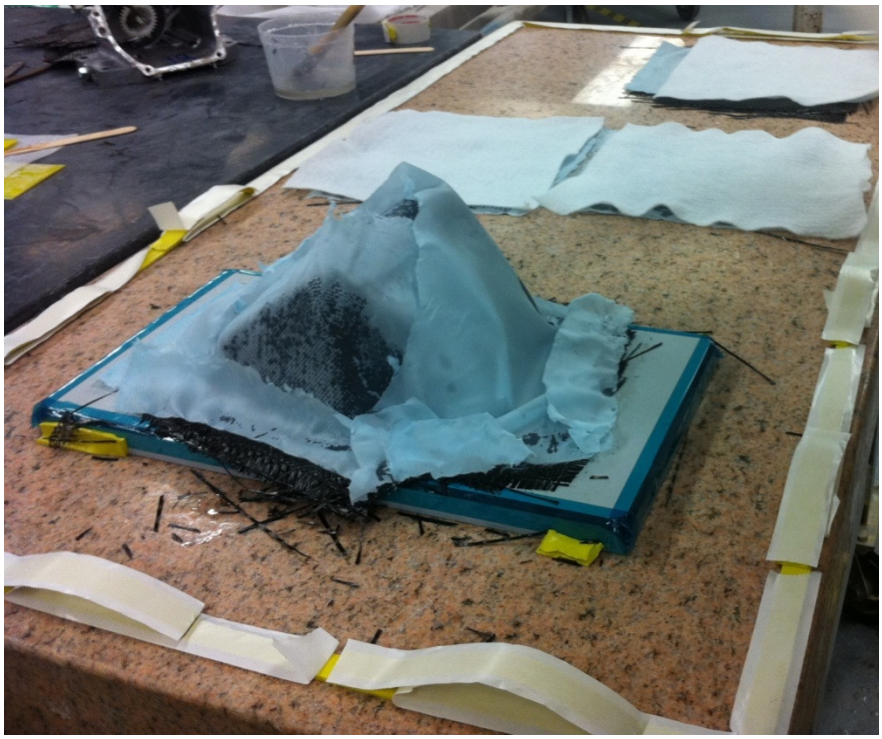

Figure 41: Wet Layup of Crankcase (Foreground) and Crankcase Test Panels (Background)

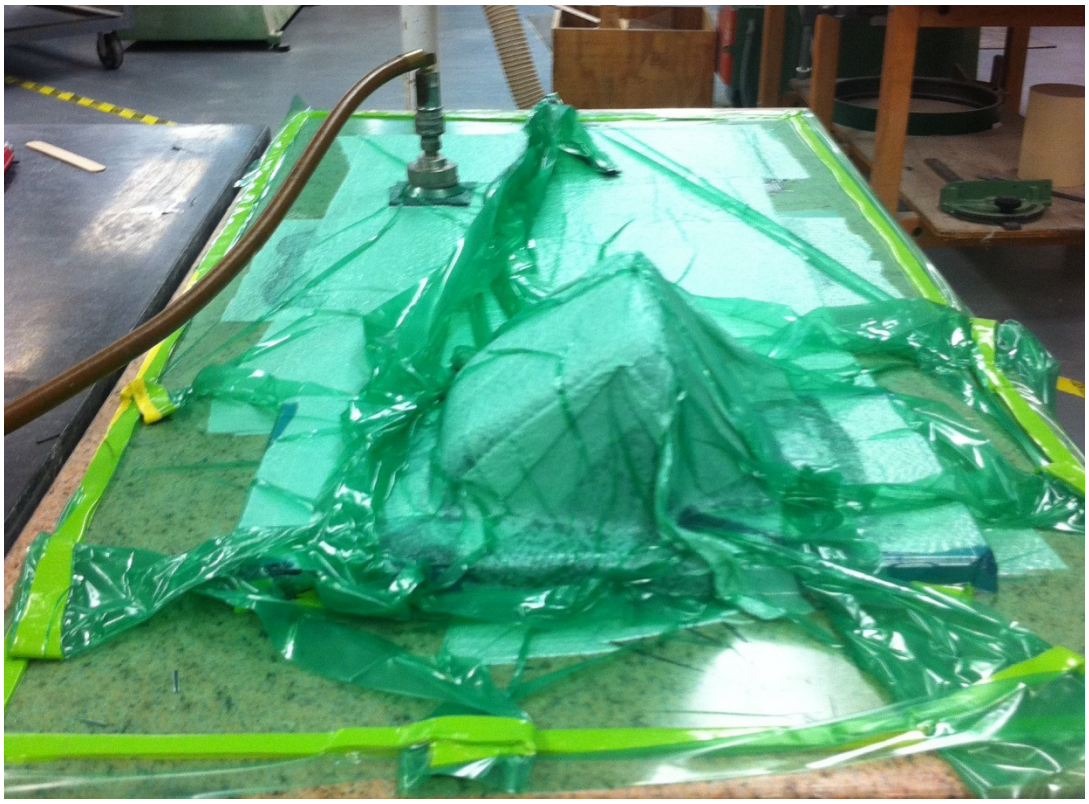

Figure 42: Vacuum Bagging of the Room Temperature Cure Crankcase and Test Panels

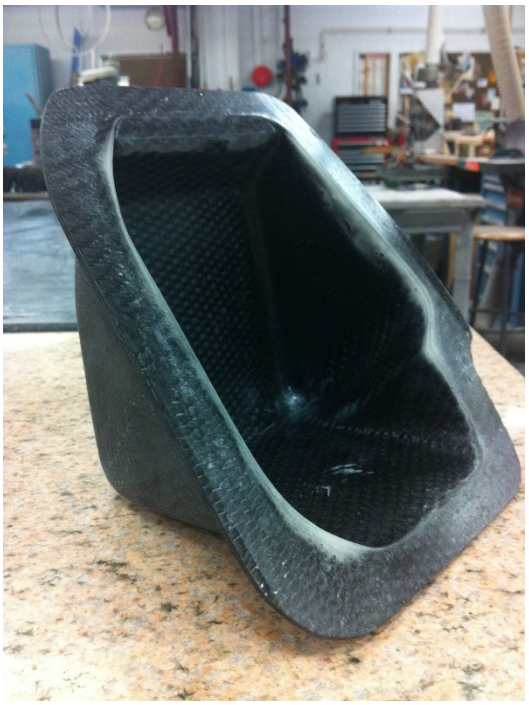

Figure 43: Room Temperature Cure Crankcase

Figure 44: Aluminum Crankcase and CFRP Crankcase Comparison

Figure 45: Naval Academy Autoclave

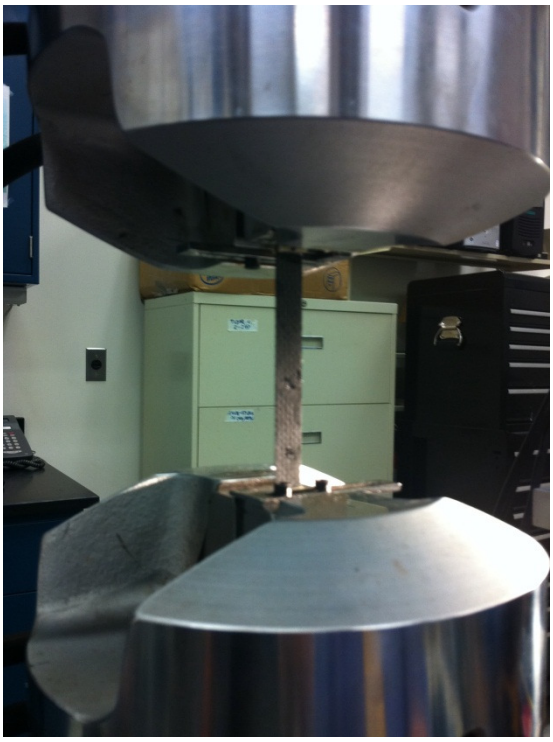

Figure 46: Material Testing Setup using Tensile Test Equipment

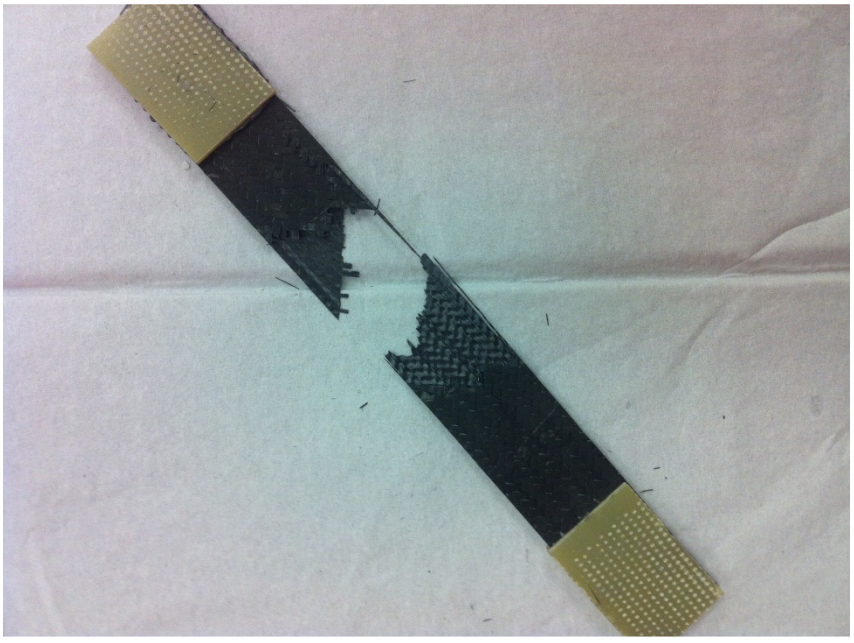

Figure 47: Tensile Specimen used to Calibrate FEA Models

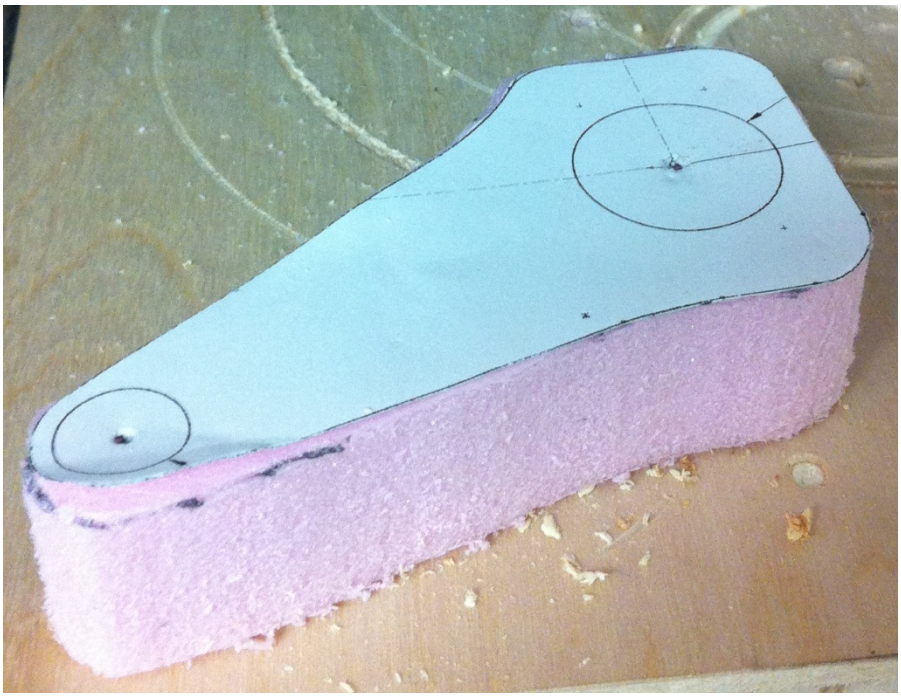

Figure 48: CFRP Connecting Rod Profile Foam Model

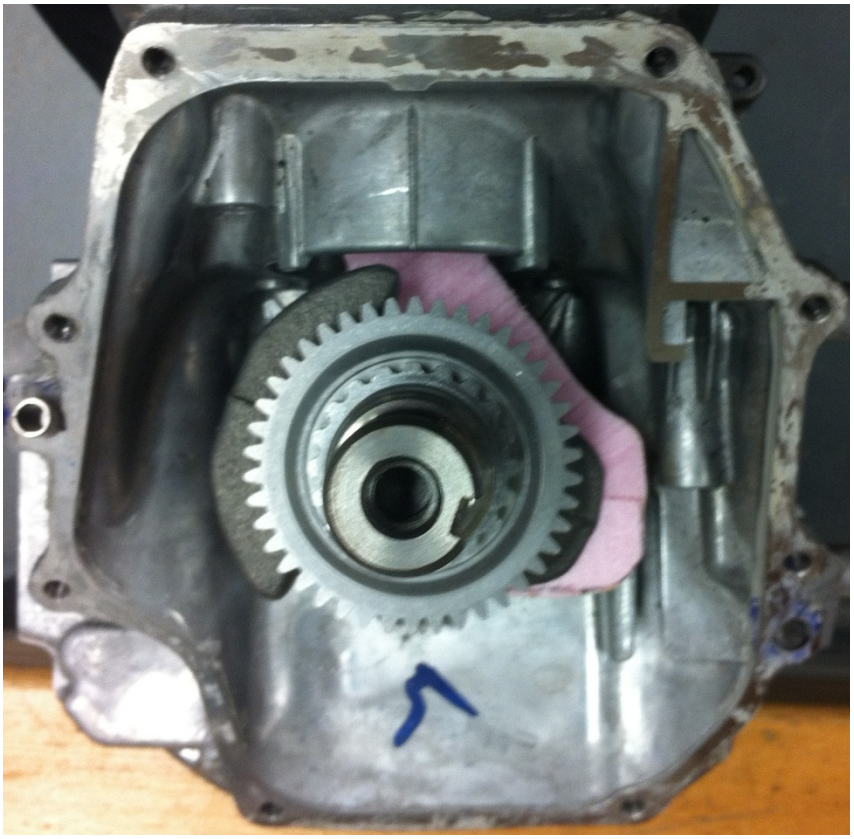

Figure 49: Foam Connecting Rod Testing for Clearance

Figure 50: CFRP Crankcase Fitting to Upper Portion of Engine

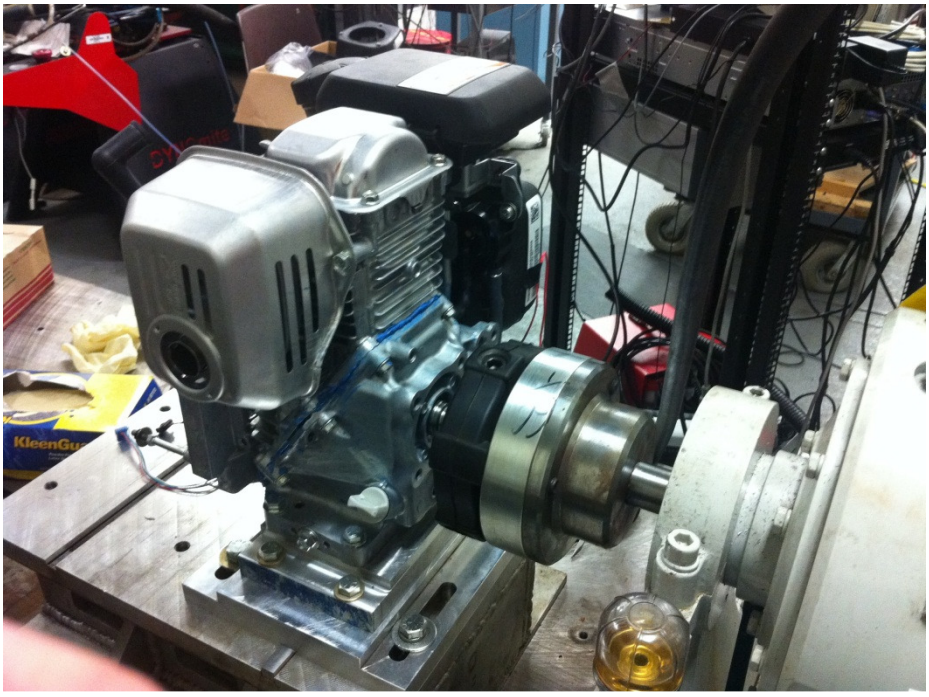

Figure 51: Experimental Setup

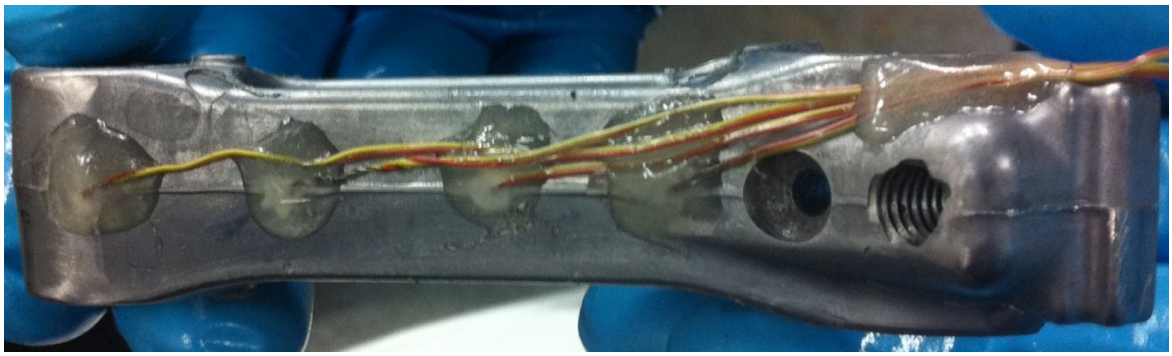

Figure 52: Wired K-Type Thermocouple Setup for Connecting Rod

Figure 53: Epoxy Securing Points for all Wired Connecting Rod Tests

Figure 54: Failed Tests due to Wire Fatigue

Figure 55: Failed CFRP Connecting Rod due to Bearing Sizing

Figure 56: G10 Core after CFRP Connecting Rod Test

Appendix E: Detailed Instrumentation Information

E.1 Piezo-capacitive Pressure Transducer

A Kistler Type 6117 Spark plug was used to get in cylinder pressures during engine operation. The spark plug is outfitted with a piezo-capacitive pressure transducer to avoid boring a hole in the head to measure the in cylinder pressure. A piezo-capacitive crystal gives off very small voltages, on the order of pico-Coulombs, when subjected to loading (i.e. combustion pressure). This small voltage is amplified and the data is collected using LabVIEW. The LabVIEW data is used in conjunction with a Digital Shaft Encoder to fit the pressure data to the Crank Angle Degree (CAD) data. This shows where the piston is during each pressure data point.

E.2 Dynamometer

A dynamometer is used to measure the torque and power output of an engine. This allowed for engine testing to be completed in a lab to gather temperature, strain, and pressure data. The dynamometer provided resistance to the shaft and was controlled by a Dyne Systems Inter-Loc V Digital Multi-loop Controller that allowed the user to input engine speeds. As the engine speed input dropped, the resistance of the engine was increased to slow the shaft to the appropriate speed. With this control system, the engine was able to be tested at various load points (i.e. Max Power or Max Torque). The dynamometer used was a Model 66 Midwest and Dynamatic Eddy Current Dynamometer. Dynamometers can provide resistance to a shaft either by using a water pump or by using electrical current to create a magnetic field that resists the engine's movement. A water pump dynamometer increases load simply by pumping more water. An eddy current increases load when the current through the dynamometer increases, creating a larger magnetic field. The electrical current is either dissipated through a heat exchanger device or is added to the electrical grid.

E.3 Strain Gages

Strain gages were used to gather strain data on the crankcase and the connecting rod. The strain gages used an Omega BCM-1 full Wheatstone bridge configuration connected to an Omega DMD-465WB high bandwidth instrumentation amplifier with amplification to 2 kHz (-3 dB point). The high bandwidth is unique among strain gage amplifiers, and would allow the dynamic strain signal from engine operation (cycle frequency at 3400 RPM is approximately 30 Hz), but still provide filtering for higher frequency noise created by the spark or surrounding electronic equipment. The strain data was collected with National Instruments data acquisition system using a PCI-6259 16 bit multichannel analog-to-digital converter card with a BNC-2110 breakout connector block. This data acquisition hardware was operated with National Instruments LabView software, version 8.6 and collected strain data at 1 kHz.

The strain gages used for the crankcase were placed at a right angle to one another and were matched strain gages. The right angle between the two gages prevented strain in one gage's direction from giving a reading in the other gage. Thermal expansion of the case would result in strain readings in both gages. Because the thermal effects caused the strain to increase in both gage equally, the strain caused by the crankshaft during engine operation could be isolated. However, no strain data was measured because there was no appreciable strain in the crankcase during operation.

E.4 Thermocouples and Temperature Indicators

K-Type Thermocouples were used to measure temperatures of various points around the engine, ranging from the crankcase temperature, oil temperature, and connecting rod temperature. A thermocouple uses two different alloy wires that are welded together at a point. When the alloys are exposed to a temperature change, a small voltage is produced as each alloy expands at a different rate. This voltage change is correlated to a temperature change that can be recorded with data analysis equipment. Temperature data was recorded using a National Instruments SCXI-1000 and SCXI-1102 thermocouple module. This data acquisition hardware was operated with National Instruments LabView software, version 8.6, and collected temperature data at 1 Hz.

E.5 Tensile Tester

Tensile testing apparatuses were used to pull tensile specimens to failure. This enabled strength data and Young's Modulus values to be calculated. A MTS 20kip tensile stand with Flex Test Control Software and an Instron/Instrumet tensile stand with an Instron oven were used for various tests. The MTS 20 kip tensile stand used hydraulic grips to hold the specimen throughout the duration of the test. This allowed for grip pressure to be preset. The Instron/Instrumet tensile stand used grips that increased gripping force as the axial load increased. While this prevented higher loads from causing the specimen to slip, it could result in crushing the specimen before failure was achieved due to the axial load. A high temperature Instron extensometer was used to measure the strain in the samples through a large range of temperatures. The extensometer uses a gage length of exactly one inch, making strain measurements equal to the distance that the extensometer moved throughout the duration of the test. An Instron oven was used with the Instron/Instrumet tensile stand to pull specimens at elevated temperatures.

Appendix F: Heat Transfer Model Code

This code was written for Engineering Equation Solver. The aluminum model was used to calibrate how much combustion energy is transferred to each node along the cylinder. These correction coefficients were to be used to correct the heat transfer energy in the CFRP model. Unfortunately this model was unable to yield realistic results.

```
"Heat Transfer Equations"
"Mark Trunzo"

q=3725 [W] "The energy transferred for each combustion cycle. This represents the maximum power of the engine and can be assumed to be the heat energy lost due to the 1/3 rule"
T_inf=25 [C] "ambient air temperature"

T_head=110 "defined by experimental results"

"The following block assigns the temperatures in the equations to an arrays table"
T_1=T[1]
T_2=T[2]
T_3=T[3]
T_4=T[4]
T_5=T[5]
T_6=T[6]
T_7=T[7]
T_8=T[8]
T_9=T[9]
T_10=T[10]
T_11=T[11]
T_12=T[12]

"The following block assigns each node a temperature that was measured during engine operation"
T_1=112
T_2=120
T_3=124
T_4=126
T_5=128
T_6=129
T_7=131
T_8=131
T_9=115
T_10=104
T_11=117
T_12=122

"The Following block has the resistance values for conduction, convection, fin geometry, and junction contact. The last three represent CFRP resistances"
R_cond=.01209
R_conv=0.256495
R_f=.080876
R_contact=2.642106
{R_inweave=.288546
R_weave=5.775006
R_convw=.617284}
```

"Nodes exposed to combustion gases"
"The c values are correction coefficients that correct the each transfer for each node to what is required to model the experimental results. These coefficients are to be used in the CFRP node to model how much energy enters each node above the crankcase junction"
c1*q=(T_1-T_head)/R_cond+(T_1-T_inf)/R_f+(T_1-T_inf)/R_conv+(T_1-T_2)/R_cond
c2*q=(T_2-T_1)/R_cond+(T_2-T_inf)/R_f+(T_2-T_inf)/R_conv+(T_2-T_3)/R_cond
c3*q=(T_3-T_2)/R_cond+(T_3-T_inf)/R_f+(T_3-T_inf)/R_conv+(T_3-T_4)/R_cond
c4*q=(T_4-T_3)/R_cond+(T_4-T_inf)/R_f+(T_4-T_inf)/R_conv+(T_4-T_5)/R_cond
c5*q=(T_5-T_4)/R_cond+(T_5-T_inf)/R_f+(T_5-T_inf)/R_conv+(T_5-T_6)/R_cond
c6*q=(T_6-T_5)/R_cond+(T_6-T_inf)/R_f+(T_6-T_inf)/R_conv+(T_6-T_7)/R_cond
c7*q=(T_7-T_6)/R_cond+(T_7-T_inf)/R_f+(T_7-T_inf)/R_conv+(T_7-T_8)/R_cond
c8*q=(T_8-T_7)/R_cond+(T_8-T_inf)/R_f+(T_8-T_inf)/R_conv+(T_8-T_9)/R_cond
c9*q=(T_9-T_8)/R_cond+(T_9-T_inf)/R_f+(T_9-T_inf)/R_conv+(T_9-T_10)/R_contact

"Nodes from the Junction down"

c10*q=(T_10-T_9)/R_contact+(T_10-T_11)/R_cond
c11*q=(T_11-T_10)/R_cond+(T_11-T_12)/R_cond
c12*q=(T_12-T_11)/R_cond+(T_12-T_inf)/R_conv

"These values assign each node an array to be used for graphing purposes"
Node[1]=1
Node[2]=2
Node[3]=3
Node[4]=4
Node[5]=5
Node[6]=6
Node[7]=7
Node[8]=8
Node[9]=9
Node[10]=10
Node[11]=11
Node[12]=12

Glossary

A

After Top Center (ATC): The position of the crankshaft when the piston is at the highest point in the stroke.

Autoclave: A pressure capsule that uses vacuum pumps to pull a vacuum on a CFRP part while also applying an external pressure during the cure process. Elevated temperatures can also be applied during the cure process.

D

Debulk: The process of removing all excess air from a vacuum bag with a vacuum pump during the cure process.

Dynamometer: An instrument that measures engine torque and power outputs while also controlling engine speed with mechanical or electrical resistance.

F

Factor of Safety: The ratio of the maximum force a part can withstand and the force the part is expected to operate under.

Flash Point: The minimum temperature for a fuel to begin to vaporize and become a combustible gas.

H

Heat Transfer Model: A model of nodes that are connected by thermal resistance values. Given an amount of energy that will travel through the system, a heat transfer model can predict the temperature at each node.

I

Irreversible Chemical Temperature Indicators: Indicators applied to a surface that change color once a minimum temperature is reached and do not change back when the part is cooled.

L

Liquid Shim: A liquid pad that is used to align a part while also maintaining contact with a securing point such as a wall.

M

Modulus of Elasticity: A material property that is defined by the slope of a stress/strain curve. It represents the materials tendency to be deformed.

Mold: A solid object that holds carbon fiber weaves in place when subjected to a vacuum during the cure process.

P

Power Density: A normalized measure of an engine's power output. Calculated by taking the engine weight over the power output.

Power to Weight Ratio: See Power Density

Pre-Impregnated Weave: A weave of carbon fiber that is manufactured with the appropriate amount of resin in the fibers. This type of CFRP must be cured at elevated temperatures.

R

Room-Temperature Vulcanizing (RTV) Gasket-Making Paste: A paste that is used to seal engine crankcases.

S

Strength-to-Weight: Normalized material strength, calculated by taking the ultimate or yield strength over the weight of the part.

T

Thermal Conductivity: A material's ability to conduct heat.

Top Dead Center (TDC): The position of the piston at the highest point in the stroke.

V

Vacuum Bagging: The process of sealing a CFRP part in a bag and pulling a vacuum to remove all excess air. This process can be done both at room temperature and in an autoclave.

Young's Modulus: Represents a material tensile property that is used to quantify stiffness.

#

1/3 Rule: A guideline to determine how much energy from fuel injected into the combustion chamber is converted to work to drive the piston, heat transferred out of the cylinder, and enthalpy in the exhaust gases. 1/3 of the fuel energy is converted equally into each of the aforementioned values.

50% Burn Point: The point during combustion that represents when 50% of the fuel has been combusted.